REVIEW

Check for updates

2D nanostructures beyond graphene: preparation, biocompatibility and biodegradation behaviors

Shige Wang, [ID] [abc] Xueqing Yang,[a] Lingling Zhou,[a] Jinfeng Li[a] and
Hangrong Chen [ID] *[b]

Much attention has been paid to the fabrication of two-dimensional (2D) nanomaterials as therapeutics for nanomedicine in recent years owing to their special physicochemical characteristics. These fascinating physicochemical properties alongside their diverse biomedical applications drive us to give a review of the present endeavors of interest in these 2D nanomaterials. In this review, the up-to-date research advances of the preparation, biocompatibility and biodegradation behaviors of 2D nanomaterials including transition-metal dichalcogenides (TMDs), transition metal oxides (TMOs), black phosphorus (BP) nanosheets, metal–organic frameworks (MOFs), 2D boron (B), boron nitride (BN), layered double hydroxides (LDHs), 2D nanoscale metals, and other kinds of 2D nanomaterials are introduced. The *in vitro* and *in vivo* bio-compatibility, including their degradation assessments from the aspects of a redox reaction, enzymes, pH, and the cell environment, *etc.*, of the above categories of 2D nanomaterials are discussed in detail. Finally, the prospects and challenges of the development of 2D nanomaterials aiming for biomedical applications are summarized.

1. Introduction

As a class of brand-new nanomaterials, two-dimensional (2D) nanosheets have gained much attention in the past few decades, and dimensionality is considered to be one of the key parameters that could substantially influence the properties of certain nanomaterials.[1] Featuring ultrathin atomic thickness, large surface area, facile surface modification, controllable size, and admirable photo-to-heat conversion efficiency, 2D nanomaterials

[a] *College of Science, University of Shanghai for Science and Technology,*
No. 334 Jungong Road, Shanghai 200093, China
[b] *State Key Laboratory of High Performance Ceramics and Superfine Microstructure,*
Shanghai Institute of Ceramics, Chinese Academy of Sciences, No. 1295 Dingxi
Road, Shanghai 200050, China. E-mail: hrchen@mail.sic.ac.cn
[c] *Department of Chemistry, National University of Singapore, 117543, Singapore*

Dr Shige Wang received his PhD degree in Materials Science and Engineering from the College of Materials Science and Engineering, Donghua University, in 2013. He then worked as a Postdoctoral Fellow at the Shanghai Institute of Ceramics, Chinese Academy of Sciences, under the supervision of Prof. Hangrong Chen. He is an associate professor at the University of Shanghai for Science and Technology. His current research interests include two dimensional transition metal sulfides for nanomedicinal applications and polymer hydrogel and nanofiber-based materials for tissue engineering and cancer therapy applications.

Shige Wang

Xueqing Yang received her BS degree in Chemistry from Hefei Normal University. She is currently studying for an MS degree in Chemistry from the University of Shanghai for Science and Technology, under the supervision of Dr Shige Wang. Her research interests are in the areas of the synthesis and surface modification of nanomaterials for drug delivery.

Xueqing Yang

have been found to have broad prospects in sensing, drug carriers, and other fields. The morphologies of 2D nanomaterials could be nanoplates, nanodisks or nanosheets (NSs). Compared to zero-dimensional and one-dimensional materials, the unique 2D structure imparts many unique physicochemical properties (like a compelling quantum size effect) to such kinds of nanomaterials. These fascinating physicochemical properties along with their diverse biomedical applications drive us to give a review of the up-to-date research progress of these materials. In this review, different synthesis strategies of some typical 2D nanomaterials are summarized. Also, detailed evaluations of their biocompatibility from the perspectives of cell, blood and histocompatibility, and the biodegradation of 2D nanomaterials by enzymes and the specific responsive biodegradation in the tumor microenvironment (TME) are covered.

As the first set of 2D nanomaterials, graphene and graphene-based derivatives (especially graphene oxide (GO) as well as reduced GO, r-GO) have become a research hotspot in materials science.[2,3] Graphene could be easily exfoliated into single-layer nanosheets with functional oxygenated groups on the edges and basal planes, and thus could be further covalently functionalized with other polymers.[4] Furthermore, many kinds of inorganic
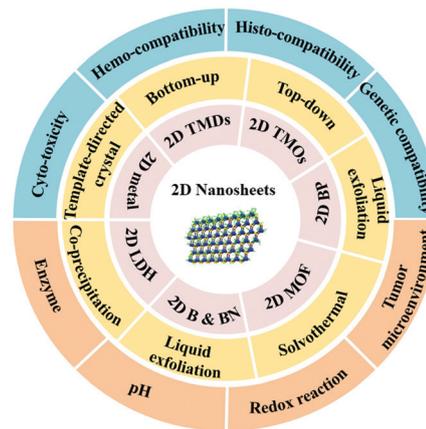
Scheme 1 The synthesis methods, biocompatibility aspects, and degradation mechanisms of different kinds of 2D biomaterials.

nanoparticles (NPs) could be successfully anchored on graphene surfaces to produce graphene-based nanocomposites for cancer therapy under the guidance of multi-modal imaging.[5] Recently, the 2D nanomaterial family has expanded from graphene and graphene-based nanomaterials to transition-metal dichalcogenides (TMDs), transition metal oxides (TMOs), black phosphorus (BP), metal–organic framework (MOFs), boron (B), boron nitride (BN), layered double hydroxides (LDHs), metal nanosheets, and 2D nanomaterial-based composites. Several cutting-edge reviews have summarized the preparation and application of GO and GO-based nanoplatforms, and the applications of some other typical 2D nanomaterials have also been extensively reviewed;[6–9] herein we summarize some major progress of the synthesis, cell response and biodegradation of typical 2D nanomaterials beyond graphene (Scheme 1).

2. Preparation of 2D biomaterials

2.1 2D TMDs

2.1.1 Top-down strategy. 2D TMDs such as MoS_2 and WS_2 are the second class of most studied plane-structured nanomaterials beyond graphene. Recently, more attention has been

Lingling Zhou received her BS degree in Chemical Engineering and Technology from Huangshan University. She is currently studying for an MS degree in Chemical Engineering from the University of Shanghai for Science and Technology, under the supervision of Dr Shige Wang and Prof. Hangrong Chen. Her research interests are in the areas of the synthesis and surface modification of nanomaterials for biomedical applications.

Lingling Zhou

Jinfen Li received her BS degree in Chemical Engineering and Technology from Panzhihua University. She is currently studying for an MS degree in Green Chemical Process and Comprehensive Utilization of Resources from the University of Shanghai for Science and Technology. Her research interests are in the areas of 2D nanomaterials and polymer synthesis and surface modification of nanomaterials for biomedical applications.

Jinfeng Li

Prof. Hangrong Chen received her PhD degree in materials science & engineering from the Shanghai Institute of Ceramics, Chinese Academy of Sciences, in 2001. Her research interests are mainly focused on nanomaterials for biomedicine and catalysis science areas, including the development of intelligent-responsive theranostic nanoplatforms, novel drug delivery systems, imaging nanoprobes, etc.

Hangrong Chen

This journal is © The Royal Society of Chemistry 2020

J. Mater. Chem. B, 2020, **8**, 2974–2989 | **2975**

focused on 2D TMDs chemically exfoliated using lithium intercalation for potential biomedical applications.[10–17] During the exfoliation, an intercalation reagent (like lithium alkylide) could diffuse thoroughly into the interlayer space of a bulk 2D TMD crystal and act as an active "molecular bomb" upon contacting water and randomly cleave the bulk crystal into fragments. In striking contrast to the bulk counterpart, the exfoliated fragments could have a monolayer structure with ultra-small size, extremely higher surface-area-to-mass ratios, abundant surface hydroxyl groups and defect sites which are favorable for further surface modification and adsorption of drugs, DNA and other small functional materials.[14,18–20] For example, Kim et al. presented an exfoliation strategy based on sonication of the bulk TMD in N-methyl pyrrolidone (NMP) by using a tip sonicator and experimentally confirmed that the exfoliated 2D TMD NSs exhibited high radical scavenging capability, and their intensities follow the order $WSe_2 > WS_2 > MoSe_2 > MoS_2$. Based on the thorough investigation of their structural characteristics, the authors predicted that the radical scavenging capability could have originated from the chalcogen defect-mediated hydrogen atom transfer in certain solutions of these 2D TMD NSs.[21] Due to the large specific surface area-associated absorbing ability and the intrinsic fluorescence quenching capacity of transition-metal ions, chemically exfoliated TMDs were chosen as nanoplatforms for the detection of DNA or RNA in bench work. As a representative example, Zhang and co-workers uncovered that single-layer MoS_2 NSs could effectively adsorb the nucleobases of a single-stranded DNA (ssDNA) probe via van der Waals force to substantially quench the fluorescence of the pre-labeled dye. When single-layer MoS_2 NSs hybridize with the complementary ssDNA, the affinity between the primary ssDNA probe and the single-layer MoS_2 NSs will be eliminated and the dye-labeled ssDNA will be separated in situ, resulting in an automatic recovery of the dye fluorescence. Such prominent fluorescence quenching and recovery phenomena could be applied for quick DNA sequencing.[18] Zhang et al. fabricated a series of metal sulfide NSs by exfoliation of layered structured bulk metal sulfides using a common photochemical approach. The laminar structure of the precursor guides the formation of metal sulfide NSs, while the photoirradiation allows the precursor to break down controllably at an appropriate temperature without changing its 2D structure. Using this strategy, PbS NSs with good crystallization and a thickness of 1.4 nm were successfully synthesized. This photo-induced top-down method could also be used for the successful one-pot synthesis of CdS, Cu_9S_5, wurtzite $CuInS_2$, and Cu_2SnS_3 NSs.[22]

Besides, top-down synthesized 2D TMDs could be further used as templates to prepare 2D TMD based nanocomposites. For instance, intercalation-exfoliated MoS_2 NSs were used as substrates to support the formation of AuNPs@MoS_2 nanocomposites with a microwave-assisted hydrothermal method. The precursors used were carboxymethyl cellulose and $HAuCl_4$. The reaction dynamics were based on the fact that MoS_2 could straightforwardly react with metal precursors in redox chemistry to allow green and direct redox $HAuCl_4$ to form zero-valent AuNPs. This AuNPs@MoS_2 nanocomposite was used as both an electrode modifier and a nanoamplifier for miRNA-21 detection.[23] Recently, great attention has been paid to the design of bio-materials especially 2D nanomaterials for photo-induced tumor therapy.[24–26] Yong et al. prepared bovine serum albumin (BSA)-WS_2@MB (methylene blue) nanocomposites for the combined photothermal therapy (PTT) and photodynamic therapy (PDT) of cancer. Herein, H_2SO_4 was selected to intercalate bulk WS_2 under ultrasonic stripping to obtain water- and air-inert composites. As found, the yield of such an acid assisted stripping is higher than traditional lithium-ion intercalation and the average thickness of the nanocomposites was approximately 1.6 nm.[26] In another study, Lei et al. prepared non-covalently modified hydrophilic $MoSe_2$ NSs by using polyvinylpyrrolidone (PVP) assisted peeling and encapsulated them in a poly(N-isopropylacrylamide) hydrogel. Then, an intelligent drug delivery carrier platform with both light and thermal response capabilities based on this hydrogel was fabricated for further tumor therapy. Using an improved oleum treatment exfoliation process, Yin et al. coated MoS_2 nanoplates with modified chitosan (CS) and loaded with anticancer drug doxorubicin (DOX). The prepared MoS_2-CS-DOX nanocomposites have dual functions of PTT and drug controlled release.[15] Generally, the top-down strategy is time-consuming to produce 2D nanosheets with controllable morphologies and thicknesses, and to guarantee their physiological stability, further tedious surface modifications were needed.

2.1.2 Bottom-up synthesis. The bottom-up synthetic route is an alternative way of the top-down strategy for the production of 2D TMDs since the latter is less efficient and often gives rise to products with uncontrollable morphologies and thicknesses.[27] Bottom-up synthesis usually employs certain precursors to prepare 2D TMDs in a controlled way from the molecular level. For instance, Ding et al. demonstrated a bottom-up strategy to synthesize a TMD QD library with members of $RuSe_2$, WSe_2, $MoSe_2$, $MoTe_2$, MoS_2, RuS_2, and WS_2 using TMD oxides or chlorides and sodium chalcogenides as precursors. At room temperature, the reaction could instantaneously reach its equilibrium within a duration of $\sim$10–20 s. As an exemplary case, the produced MoS_2 QDs were selected for further biomedical application evaluation, and it was found that the oxidative stress generation could be enhanced by increasing the density of sulfur defects through the photodynamic effect in cancer cells.[28] Recently, the scalable and high-yield synthesis of ternary chalcogenide NSs including Ta_2NiSe_5 and Ta_2NiS_5 NSs in a special electrochemical Li-intercalation and exfoliation way was reported in the literature.[11] Firstly, a layered Ta_2NiS_5 (or Ta_2NiSe_5) bulk compound, polyvinylidene fluoride and acetylene black were added to NMP. Then, the formed homogeneous slurry was evenly coated onto a copper substrate, which was then used as the cathode to assemble a battery cell. The anode and electrolyte is Li foil and $LiPF_6$, respectively. The lithium intercalation of the microflakes was initiated simultaneously along with the discharge process. This electrochemical Li-intercalation and exfoliation method was applied to the production of different kinds of 2D nanomaterials such as Bi_2Te_3, Sb_2Se_3, WSe_2, $NbSe_2$, ZrS_2, TaS_2, TiS_2, WS_2, MoS_2, and even BN or graphite.[29,30] Other newly emerged candidates of 2D nanomaterials include 2D magnetic iron sulfide (FeS) and copper sulfide (CuS). Liu and

2976 | J. Mater. Chem. B, 2020, **8**, 2974–2989

This journal is © The Royal Society of Chemistry 2020

co-workers synthesized FeS nanoplates by treating iron(II) acetyl-acetonate and trioctylphosphine oxide in oleylamine at a high temperature. Using a layer-by-layer polymer coating approach, the as-made FeS nanoplates were further modified with PEG to enhance their biocompatibility. The formed FeS-PEG nanoplatform was used for magnetic resonance imaging (r_2 = 209.8 mM^{-1} s^{-1}) guided tumor PTT.[31] 2D CuS nanoplates were produced with the bottom-up hydrothermal procedure, where CuSO$_4$·5H$_2$O, (NH$_4$)$_2$S and PVP aqueous solution were selected as precursors. The formed CuS nanoplates presented an average thickness of 23.8 nm and a mean edge length of 59.4 nm.[32] Meanwhile, the bottom-up solution-phase approach could also be used for the production of 2D TiS$_2$ NSs.[33]

Engineering multifunctional TMD nanocomposites by hybridizing with other materials using the bottom-up approach has been deemed as a fascinating approach to overcoming the shortcomings of individual counterparts and optimizing their performance or generating new functions.[11,33,34] For instance, Cheng and co-workers proposed a method for the high-yield production of metal ion (including Fe, Co, Ni, Mn, and Gd) doped WS$_2$ NSs by reacting sulfur (S) with MCl$_x$ (M = Fe^{3+}, Co^{3+}, Ni^{2+}, Mn^{2+}, and Gd^{3+}) and WCl$_6$ in an oleylamine and 1-octadecene mixture solution under a N$_2$-protected atmosphere at 300 °C. During the reaction, the metal precursors and tungsten will first form a complex with oleylamine and then react with S to form a flake-like composite. Scanning transmission electron microscopy (SEM) and energy-dispersive X-ray spectroscopy mapping suggested a homogeneous doping of metal ions inside the WS$_2$:Mn$^+$ NSs. Subsequent surface modification of C18PMH-PEG was carried out to endow the nanoflakes with colloidal stability under physiological conditions.[35] We recently presented a general method to produce 2D PEGylated MoS$_2$/MS$_x$ composite NSs (M = Bi, Cu, Pd, and Zr) by solvothermal treatment of (NH$_4$)$_2$MoS$_4$ and PEG-400/water dispersion containing certain salts (e.g., Bi(NO$_3$)$_3$·5H$_2$O, Cu(NO$_3$)$_2$, potassium tetrachloropalladate (K$_2$PdCl$_4$) and Zr(NO$_3$)$_4$·5H$_2$O). During the synthesis, PEG-400 chains were surface-coated on the composite NSs to give them colloidal stability.[27] In a later study, the Liu group reported the synthesis of Bi$_2$Se$_3$ NSs decorated with mono-dispersed FeSe$_2$ nanoparticles (FeSe$_2$/Bi$_2$Se$_3$ NSs) with a cation-exchange method. The FeSe$_2$/Bi$_2$Se$_3$ NSs were further functionalized with a PEG-grafted amphiphilic polymer for tetra-modal image-guided tumor radiation and PTT.[34]

2.2 2D TMOs

Single- or multi-layer TMOs have a relatively long history than other atomically thin materials. TMOs are highly tunable owing to the diversity of their chemical compositions, crystal structures and relative ease of inducing oxygen defects. Compared with their bulk counterparts, 2D TMOs often exhibit different physical and chemical properties.[36] Similarly, 2D TMOs could be produced via either bottom-up or top-down procedures. Among the 2D TMOs, 2D MnO$_2$ is one of the most frequently studied ones in biomedicine. Being interlayer cations sandwiched with metal oxide monolayers, 2D MnO$_2$ exhibits strong cation-exchange properties and facile redox activity.[37] In a

previous study, 2D MnO$_2$ NSs were exfoliated in H-MnO$_2$ (prepared by exchanging the Na$^+$ of layered Na-MnO$_2$ materials with H$^+$) tetrabutylammonium hydroxide solution to construct a 2D MnO$_2$ NS based theranostic platform with high dispersity and ultrasensitive pH-responsive drug release/delivery and imaging capacity.[38] It was found that the 2D MnO$_2$ NSs could break up under a TME mimicking acidic conditions, to produce Mn^{2+} ions and enhance the imaging performance at both cell and animal levels. Like other 2D NSs, the MnO$_2$ NSs could also serve as a cargo carrier to load different therapeutics. For example, Min et al. developed a novel targeted bioimaging and tumor PDT system using folic acid (FA)-modified MnO$_2$ NSs to load zinc phthalocyanine (ZnPc, a photosensitizer).[39] Ultrathin MnO$_2$ NSs have also been used for label-free biosensing applications. To this end, MnO$_2$ NSs were synthesized by mixing MnCl$_2$·4H$_2$O and tetramethylammonium hydroxide and H$_2$O$_2$ solution.[40] Chen and co-workers synthesized a series of ultrathin 2D MnO$_2$ nanosheets (M-NSs) using a "wet-chemical" synthesis method with the assistance of BSA. The formed M-NSs were then functionalized/stabilized with a unique "sono-chemical" approach (Fig. 1a). In this study, the authors suggested that the diameter and thickness of the NSs could be adjusted by altering the ratio of BSA to Mn^{2+} (Fig. 1b and c). They found that M-NSs with smaller size and thinner thickness showed better photothermal conversion and glucose oxidase-like catalytic activity. M-NSs could transform the glucose into gluconic acid and H$_2$O$_2$ to initiate glucose deprivation for cancer starvation, while M-NS-mediated PTT could efficiently eradicate tumors via hyperthermia.[41]

A MnO$_2$-based 2D "glycocluster" was used to load Chlorin e6 (Ce6, a kind of photosensitizer) and was found to be exclusively taken up by triple-negative breast cancer cells that overexpress mannose receptors. Besides, glutathione (GSH)-caused intracellular material degradation could enhance the fluorescence of the photosensitizer to realize tumor PDT under magnetic resonance imaging guidance. In this study, a 2D glycocluster
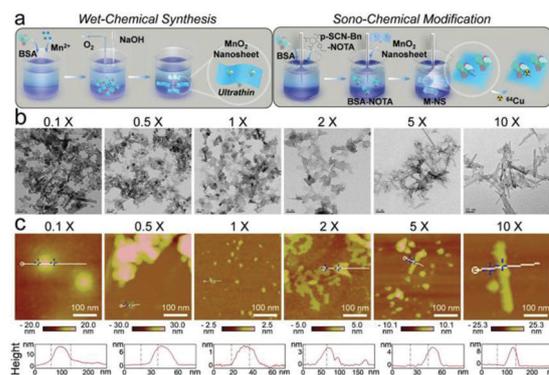

Fig. 1 (a) Scheme of the two-step synthesis of M-NSs: BSA directed "wet-chemical" method synthesis and "sono-chemical method" surface modification of the M-NSs. (b) TEM images (scale bar = 50 nm) and (c) AFM images and height mappings of the M-NSs under the guidance of BSA. The "10×", "5×", "2×", "1×", "0.5×", and "0.1×" represent BSA doses of 60, 30, 12, 6, 3, and 0.6 mg, respectively (scale bar = 100 nm). Reprinted from ref. 41. Copyright 2019 John Wiley & Sons.

This journal is © The Royal Society of Chemistry 2020

J. Mater. Chem. B, 2020, 8, 2974–2989 | 2977

was prepared by self-assembly between a glycoprotein mimetic and top-down exfoliated 2D MnO$_2$.[42] Li *et al.* prepared MnO$_2$ NSs by oxidizing manganese chloride in tetramethylammonium hydroxide/H$_2$O$_2$ in an ultrasonic bath. The formed MnO$_2$ NSs were modified with PEG ring arginine–glycine aspartic acid tripeptide (PEG-cRGD) and used as photothermal agents and nanocarriers to encapsulate Ce6 for targeted tumor therapy.[43]

Other categories 2D TMOs including MoOx and ZnO *etc.* were also systematically prepared. Liu and co-workers prepared molybdenum oxide NSs with surface PEG modification (MoOx-PEG), by treating the precursor of ammonium molybdate in a hydrothermal route. The MoOx-PEG NSs had a strong NIR absorbance capacity and could effectively load therapeutic molecules onto their surfaces to realize tumor chemotherapy and NIR-triggered tumor PTT.[44] In another study, Zhai and co-workers synthesized MoOx NSs using the same one-pot hydrothermal approach. To achieve physiological stability under physiological conditions and improve their biocompatibility, the as-synthesized MoOx NSs were surface modified with Pluronic F127. The stability of MoOx@F127 NSs was confirmed by incubating MoOx@F127 NSs with serum and PBS at different pH values to mimic the TME and physiological conditions.[45] PEG-coated and FA-functionalized zinc oxide (FA–PEG–ZnO) NSs were also successfully designed to act as a potential platform for biomedical applications.[46]

2.3 2D BPs

BP has increasingly attracted scientific attention since its first applications in biomedicine due to its unique properties and excellent biocompatibility.[47] In the monolayer BP structure, every P atom is covalently bonded with the other three P atoms. These P atoms form a bilayer structure and folded structure along the zigzag direction and the armchair direction, respectively, by van der Waals interactions. 2D BP NSs or quantum dots (QDs) are suitable for fundamental research as either photosensitizers for efficient singlet oxygen generation or theranostic agents for imaging-guided PTT. Based on the excellent dispersity of bulk BP powder in NMP, Chu *et al.* recently suggested a novel liquid exfoliation synthesis, namely, a combined bath sonication and probe sonication approach from bulk BP. The formed 2D BPQDs presented a thickness of 1.5 nm and a diameter of 2.6 nm. The ultra-small BPQDs are photo-stable and exhibit an excellent NIR light-induced photo-to-thermal conversion efficiency, with an extinction coefficient and a photothermal conversion efficiency of 14.8 L g^{-1} cm^{-1} and 28.4%, respectively, upon exposure to an 808 nm NIR laser.[48] In another research study, a bulk BP material was also exfoliated in NMP with a water bath ultrasonication process at a low temperature. The obtained precipitate was further purified by centrifugation to harvest BP NSs.[49] Using a simple modified liquid exfoliation of bulk BP in NMP, Zeng *et al.* designed a new multifunctional co-delivery system based on BP NSs exfoliated from bulk BP for targeted chemo/gene/photo-thermal treatment of multidrug-resistant tumors. In this study, DOX with a loading content of 8.2% and permeability glycoprotein siRNA with an adsorption quantity of about 4.62 nmol mg^{-1} were introduced as model therapeutic substances. Polydopamine was modified on the surfaces of BP NSs to enhance its photothermal

performance and ambient stability. In order to achieve colloidal stability under physiological conditions, NH$_2$-PEG-Apt was further conjugated onto the BP NSs' surfaces by the Michael addition reaction.[50] Using an ameliorated liquid exfoliation method, Han and co-workers successfully synthesized different kinds of BP NSs with tunable lateral sizes (*i.e.*, 4.5 ± 0.6 nm, 118 ± 22 nm, and 391 ± 75 nm). Findings in this report evidenced that the ultrasound duration and the centrifugal rate were two dominant factors in determining the size of the product.[51] Recently, researchers proposed a modified mechanical exfoliation approach using O$_2$-free water as the intercalating reagent for the synthesis of BP NSs from bulk BP powder. The produced BP NSs were then electrostatically modified with PEG-NH$_2$ to guarantee their physiological stability and biocompatibility. Furthermore, BP-PEG NSs were used to load DOX and Cy7 for NIR imaging-guided chemotherapy of tumors. And the tumor-targeting ability was introduced by conjugating FA with surface PEG (Fig. 2a, b, and g). The mean lateral size and thickness of BP NSs is about 120 nm (Fig. 2a and c) and 1–2 nm (Fig. 2e), respectively. After the surface coating of PEG-NH$_2$, the mean lateral size of BPPEG NSs decreases to 100 nm owing to the additional sonication (Fig. 2b and d). In addition, the coating of PEG could also lead to a mild thickening of $\sim$2–3 nm (Fig. 2f). Moreover, the as-prepared BP NSs with surface PEG modification could be efficiently used as the vehicles to carry drug molecules (Fig. 2h and i).[52]

Besides surface modification, BP NSs could also be substantially blended with organic substances to form composites. For example,
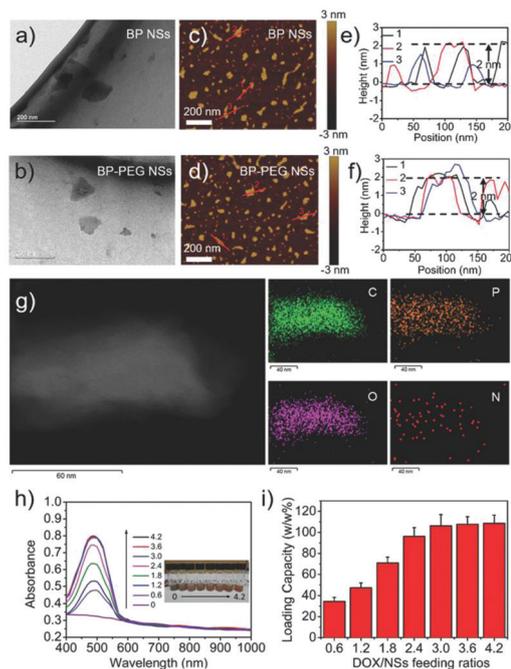

Fig. 2 (a) TEM and (c) AFM images of BP NSs; (b) TEM and (d) AFM images of BP-PEG NSs (scale bar = 200 nm); (e) AFM measured thickness of BP NSs; (f) AFM measured thickness of BP-PEG NSs; (g) STEM (scale bar = 60 nm) and EDS mapping (scale bar = 40 nm) of BP-PEG-FA NSs; (h) UV-vis–NIR spectra of BP-PEG/DOX NSs (the inset shows the varied DOX/NS feeding ratios); and (i) drug loading capacities of DOX on BP-PEG NSs with different DOX/NS feeding ratios. Reprinted from ref. 52. Copyright 2017 John Wiley & Sons.

Wang and co-workers produced a NIR light-triggered drug delivery platform that was fabricated by incorporating BPs and $SrCl_2$ into PLGA microspheres by an oil-in-water emulsion solvent evaporation method for bone regeneration.[53] In another research study, Qiu et al. reported the coating of mechanically-exfoliated ultrathin BP NSs with agarose gel, and the therapeutic drug DOX was encapsulated within the hydrogel matrix upon gel formation.[54]

2.4   2D MOFs

As a novel class of crystalline and porous materials formed by metal nodes and polydentate ligands, MOFs have emerged as a class of promising biomaterials due to their unique properties originating from their ultrathin thickness and large surface area with highly accessible active sites in recent years.[55,56] The general "top-down" and "bottom-up" strategies could be employed to synthesise MOF NSs. As a proof-of-concept approach, surfactant-assisted large-scale synthesis of 2D MOF NSs with a thickness of sub-10 nm has been proposed.[57] In brief, $M(NO_3)_2$ (M = Zn^{2+}, Co^{2+}, Cd^{2+}, and Cu^{2+}), pyrazine and PVP were dissolved in DMF and ethanol in a capped vial. Then tetrakis(4-carboxyphenyl)porphyrin (TCPP) ligands dissolved in a mixture of DMF and ethanol were added dropwise under stirring. After a 10 min sonication and 16 h heating at 80 °C, M (M = Zn^{2+}, Co^{2+}, Cd^{2+}, and Cu^{2+}) based 2D MOFs were successfully produced. In another study by the same group, Co, Cu, and Zn were used as metal nodes for the surfactant-assisted preparation of M-TCPP(Fe) NSs (where M = Co, Cu, and Zn). The as-synthesized 2D M-TCPP(Fe) NSs could be assembled into multilayer films on electrodes to realize the highly efficient detection of H_2O_2 and tracking of intracellular H_2O_2 of live cells.[58] To obtain 2D Cu-MOF NSs via the "top-down" method, Cu-MOF crystals were added to distilled water and stirred for 9 h for physical exfoliation (Fig. 3a and b). The Cu-MOF NSs were then used for effective inhibition of enzyme activity and control of cellular processes. An important alimentary canal-related serine protease with a well-characterized
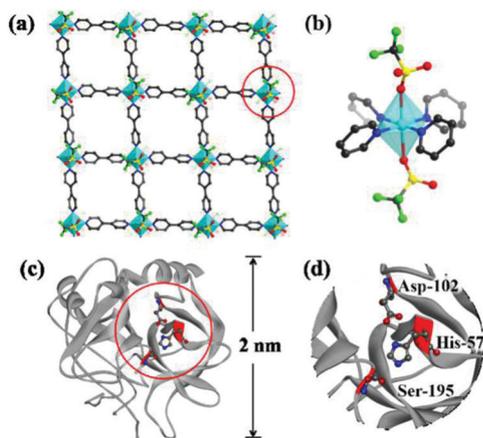

Fig. 3   (a) Schematic illustration of single-layered Cu–MOF NSs. The gray, red, green, blue and yellow parts represent the C, O, F, Cu, and S atoms, respectively. (b) Schematic illustration of central Cu(II) atoms. (c) Molecular structure of ChT. (d) Schematic illustration of the active site with residues Ser-195, His-57, and Asp-102. Reprinted with permission from ref. 59. Copyright 2017 American Chemistry Society.

structure (Fig. 3c and d), α-chymotrypsin (ChT) was selected as a model enzyme. It was demonstrated that 2D $Cu(bpy)_2(OTf)_2$ NSs could effectively inhibit enzyme activity by 96.9%, while the inhibitory effect of $Zn_2(bim)_4$ NSs was not significant. The inhibitory effect originated from the binding and coordination interactions between the enzyme and the central Cu(II).[59] Later, drug-containing MOF NSs in which Zn^{2+} ions acted as nodes and the drug ibuprofen acted as a ligand were synthesized by solvothermal treatment of a mixture containing $Zn(CH_3CO_2)_2$, ibuprofen, azobenzene, sodium dodecyl benzene sulfonate, and ethyl alcohol/deionized water in a Teflon-lined stainless steel container for 72 h. The obtained MOF NSs exhibited a remarkable pH-controlled ibuprofen release.[60] Other kinds of MOF-based multifunctional nanoplatforms like chemotherapeutic loading ones were also reported. For example, Liu et al. exploited Zn-TCPP@PEG as a drug delivery carrier for the in vivo combined chemo-photodynamic therapy of tumors.[61]

2.5   2D B and BN

2D boron (B) NSs have been produced with high-quality and in high-yield from commercial boron powder using combined liquid exfoliation and thermal oxidation etching technology. The underlying mechanism of B NS synthesis is that the B–B units on the thick layers produced in the first liquid exfoliation could be oxidized in air at high temperature to B_2O_3. This B_2O_3 could be easily dissolved into water by forming BO_3^{3-} with the second liquid exfoliation. To further improve the biocompatibility and dispersity of the resultant B NSs, they were then electrostatically modified with PEG-NH_2.[62] The BN NSs, as a novel member of 2D nanomaterials with a wide band gap, have been regarded as another typical structural analogue of carbon materials. It has a fascinating name, "white graphene", in which C atoms are substituted by N and B atoms.[63] Due to its unique honeycomb lattice structure, BN exhibits many attractive properties such as high mechanical strength, temperature stability, thermal conductivity, large specific surface area, and a low fluorescence quenching ability.[64] The 2D BN NSs with such advantageous properties have found many opportunities in biomedical applications.[65–67] Kumar et al. synthesized BN nanoflakes on a tungsten substrate using copper sulphate as the catalyst which was electrically deposited onto the substrate surface. The precursor used for BN nanoflake fabrication was boric acid and then it was heated in a tubular tube.[68] Gnatyuk et al. prepared 2D BN NPs using liquid exfoliation of the preliminary solvent-free mechano-chemically delaminated bulk h-BN. In detail, h-BN powder and NaCl crystal used as the delamination agent were mechanochemically ball-milled in an argon atmosphere. Then, the delamination agent NaCl was removed using water to obtain nanostructured h-BN (nh-BN). The preparation of 2D BN was finalized by ultrasonic disintegration in water. 2D BN materials were used as spectral markers, weak luminescent markers, and protective anticancer drug delivery systems.[69]

2.6   2D LDHs

2D LDHs are a class of clay nanomaterials that consist of positively charged and stacked brucite-type octahedral metal

hydroxide layers.[70] 2D LDHs feature a unique sandwich structure with water molecules and anions occupying the interlayer space, tunable particle size, excellent biocompatibility, a high ion exchange ability, *etc.*, thereby catching ever-increasing attention of researchers worldwide.[71] The general formula of LDHs could be represented by eqn (1):

$$[M_{1-x}^{2+}M_x^{3-}(OH)_2]^{x+}[A^{n-}]_{x/n}\cdot mH_2O \qquad (1)$$
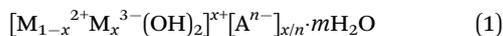
where M^{3+} and M^{2+} indicate the trivalent and divalent layer cations respectively. A^{n-} represents the exchangeable anion, and stable LDH phases are only produced by controlling the x value in the range of $0.2 < x < 0.33$ and the M^{2+}/M^{3+} ratio ranges from $2:1$ to $4:1$.[72] Gu and co-workers reported a facile three-step synthesis method to simultaneously realize the fabrication and PEG molecule conjugation of delaminated LDH NSs.[73] In another study, Shi *et al.* reported the preparation of a gadolinium (Gd)–LDH nanohybrid by hydrothermally treating a mixed solution of $Gd(NO_3)_3$, $Al(NO_3)_2\cdot 9H_2O$ and $Mg(NO_3)_2\cdot 6H_2O$ with $NaOH/NaHCO_3$ (Fig. 4a). The resultant Gd-LDH nanohybrid was proved to be able to anchor Au NPs on the surface (Fig. 4b and c). In addition, the interlayer space of the obtained nanocomposite shows a high anticancer drug loading capacity, and the introduced Au and Gd endowed the nanohybrid with excellent CT and T1-weighted MR and CT imaging capabilities (Fig. 4a).[74]

Another feature of LDHs is that it could be easily functionalized with a silane coupling reagent (such as (3-aminopropyl)triethoxysilane, APS) to introduce amine ends to afford a further conjugate with other kinds of functional groups. The main point of surface modification of LDHs was also to extend its application fields.
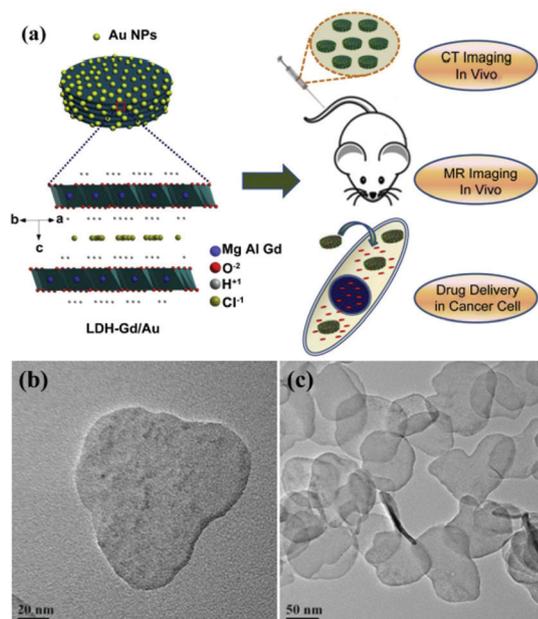

Fig. 4 (a) Scheme of the synthesis of a multi-functional LDH-Gd/Au nanocomposite for CT-MR dual-modal imaging and anti-cancer drug delivery. (b and c) TEM images of LDH-Gd/Au NSs. Reprinted from ref. 74. Copyright 2013 Elsevier B.V.

For instance, Choy *et al.* modified methotrexate (MTX)/LDH nanohybrids with APS and further conjugated with the carboxyl groups of FA. The FA modified MTX/LDH nanohybrids show an increased selectivity to cancer cells that overexpress FA receptors.[75] Shang *et al.* proposed an exfoliation of Ni-Al LDH 2D NSs through an acetone mediated aqueous miscible organic solvent treatment (AMOST) route. At 200 °C under dry conditions, the AMOST produced material could lead to superior CO_2 adsorption to conventionally reported commercial Mg-Al LDH.[76]

2.7 2D metals

Pd NSs are the most representative member of the metal NS family. To date, Pd NSs have shown excellent biocompatibility and can be easily modified.[77] Certain kinds of therapeutic agents like photosensitizers have also been successfully coated onto Pd surfaces.[78,79] Attributed to the Pd NS-mediated tumor PTT and the photosensitizer Ce6 induced photodynamic destruction effect, these as-prepared nanocomposites hold significant promise for potential multimode cancer therapies. Pd NS based composites were also designed to extend their biomedical applications. For example, Fang *et al.* designed the synthesis of Pd NS-covered hollow mesoporous silica NPs. In this research, hollow mesoporous silica spheres (HMSS) were first synthesized by using cetyltrimethylammonium bromide (CTAB) as the template and etched with Na_2CO_3 solution. The formed HMSS were then treated with 3-aminopropyltrimethoxysilane to yield HMSS-NH_2 NPs. Pd NSs were finally used to cover the surfaces of the HMSS-NH_2 NPs by virtue of their electrostatic and coordination interactions with amino groups. The formed nanocomposite could exert a therapeutic effect with minimal side effects. Therein, the hollow mesoporous silica spheres could load anticancer drugs, while the surface anchored Pd NSs could convert NIR laser light into thermal energy to realize combined tumor chemotherapy and PTT.[80] In another study, Chen and co-workers developed Pd NS coated mesoporous silica for the co-delivery of photosensitizers and small Pd NSs. In this formulation, tetra-substituted carboxyl aluminum phthalocyanine (AlC$_4$Pc) was covalently conjugated to a mesoporous silica network, while small Pd NSs were coated onto the surface *via* electrostatic interaction and coordination, to produce a nanoplatform for combined tumor PDT and PTT.[79] Beyond monometallic Pd NSs, other noble metals could also epitaxially grow over the surfaces of Pd NSs and form well-defined bimetallic nanoplates such as Pd@Ag[81] and Pd@Au NSs.[82] Zheng *et al.* designed a PEGylated Pd@Au nanoplate based drug delivery system to covalently bind the platinum(IV) prodrug c,c,t-[Pt(NH$_3$)$_2$Cl$_2$(O$_2$CCH$_2$CH$_2$CO$_2$H)$_2$] for the combined PTT and chemotherapy of tumors.[82]

Certain polymers such as functionalized polystyrene (PS) spheres or CTAB micelles could be used as a template for synthesizing 2D metal NSs.[83–85] For example, Schatz and co-workers reported the synthesis of silver nanodisks using carboxylate-functionalized PS spheres as a template. They postulated that Ag ions could electrostatically bond to the surface carboxyl groups of the PS spheres, which may block the growth of the Ag crystal in one direction and effectively guide the growth in another

(lateral) direction.[83] In another study, Wang and co-workers prepared a kind of transferable Au NS *via* the diffusion-limited aggregation approach. The SiO₂ NS template was synthesized by hydrolyzing TEOS in aqueous solution and used to adsorb $AuCl_4^-$ ions, which were finally controllably reduced to form 2D Au/SiO₂ NSs.[86] Other kinds of 2D metal NSs that have been generally studied are Gd, tellurium (Te), manganese (Mn), titanium (Ti), *etc.* Gd NSs show a high specific area and could be used as a robust clinical tool for diagnosis and imaging-guided disease therapy. In recent research, Zhang *et al.* synthesized Gd-labeled dendrimers, which were further functionalized with the targeting ligand to form FA conjugated Gd-labeled dendrimers (FA-GLD). The FA-GLD were further conjugated with NHS-GO and loaded with the anticancer drugs DOX and colchicine *via* π–π interactions.[87] More recently, Lin *et al.* synthesized Te NSs *via* a facile liquid exfoliation method using Te powder as the raw material. The formed Te NSs were then functionalized with GSH to further improve their stability and biocompatibility.[88]

2.8 Other 2D nanomaterials

Shi *et al.* synthesized 2D silicene NSs (SNSs) through a wet-chemical exfoliation method. In particular, the CaSi₂ precursor was subjected to a mild oxidation process in anhydrous acetonitrile (CH₃CN) with weak oxidant iodine. The SNSs were finally completely exfoliated using liquid N₂. The high photothermal conversion capability, inherent excellent biocompatibility and ideal biodegradability of 2D silicon offer broad prospects for silicon-based nanoplatforms in further clinical applications.[89] Another novel kind of 2D ceramic biomaterial, namely, MAX ceramic biomaterials (Ti₃C₂ NSs, MXenes), was successfully synthesized based on a two-step HF etching and TPAOH intercalation process of MAX phase Ti₃AlC₂ in the same group. The Ti₃C₂ NSs were further wrapped with soybean phospholipid (SP) to achieve colloidal stability under physiological conditions to benefit their biomedical applications.[90] Ultrathin 2D porous Zn(OH)₂ NSs with a thickness of about 3.8 nm were fabricated using Cu nanowires as a substrate, and using ZnCl₂ and Na₂S₂O₃ solution as precursors. These Zn(OH)₂ NSs were surface hydrophilic because of the existence of hydroxyl (–OH) groups, and therefore they could be covalently bonded with a silane coupling reagent to introduce functional groups. The surface-functionalized Zn(OH)₂ NSs were selected as a nanoplatform to conjugate with DNA aptamers on their surfaces to form "smart" porous NSs. These "smart" ultrathin NSs showed excellent biocompatibility, obvious cellular uptake, and an outstanding pH-triggered drug release profile.[91] In a more recent study, FA modified CONs (TpASH-FA) for targeted delivery of 5-fluorouracil into tumor cells were synthesized using a sequential post-synthetic modification of TpASH, a kind of covalent organic framework which was developed based on a salt mediated Schiff condensation. This post-synthetic modification which referred to the sequential conversion of phenolic hydroxyl to alkyl hydroxyl groups, the surface alkyl hydroxyl groups to amines, and the conjugation of cellular targeting ligands could result in the simultaneous chemical delamination and functionalization of CONs.[92] In addition to inorganic NSs, certain organic NSs found their places in the 2D NS family. For example, Wang *et al.* reported the space-confined

synthesis of ultrathin polypyrrole NSs using layered FeOCl as the removable template.[93]

3. Biocompatibility and biodegradation behaviors of 2D biomaterials

Biocompatibility refers to the ability of a material to deal with cells and substances in the living body without causing any side and harmful effects. The *in vitro* and *in vivo* biocompatibility and cellular response of 2D biomaterials are indispensable for further highlighting their clinical translational potential. Moreover, their biodegradability has been frequently researched to broaden their translational potential. Typically, the biodegradation of 2D nanomaterials is closely related to their compositional components, as well as external factors. The compositional components mainly include the physicochemical features of the 2D TMDs, while the external factors could refer to the pH, moisture, oxygen content, alkalinity or acidity, enzyme, H₂O₂, redox nature, *etc.*

3.1 2D TMDs

3.1.1 Biocompatibility. The biocompatibility of 2D TMDs is related to their size and phase since they can influence their interactions with the cell membrane.[94,95] For example, it is unlikely that WS₂ and MoS₂ flakes or sheets will permeate the cell membrane because they are of similar diameter to cells (approximately 20 μm). Besides, materials larger than 100 nm in diameter typically do not undergo endocytosis by certain cells.[94,96] The biocompatibility of mechanically exfoliated and CVD-grown pristine 2D WS₂ and MoS₂ NSs can be studied from the perspectives of cytotoxicity and genotoxicity. It was found that the direct contact of HEK293f with pristine MoS₂ and WS₂ NSs, regardless of their synthetic methods, imposed no influences on the morphology of HEK293f cells. Although the mechanically exfoliated and CVD-grown pristine 2D WS₂ and MoS₂ NSs are not acutely toxic, they may still compromise cell viability by inducing oxidative stress and triggering programmed cell apoptosis. Compared with copper (positive control, a known generator of ROS), the ROS level generated by cells was significantly lowered after being incubated with TMD particulates at various concentrations for 1, 8 and 24 hours, proving that TMD did not activate programmed cell death even after 24 hours' exposure. In addition, qualitative Live/Dead fluorescence labeling assays also illustrate that the cell viability remained unaffected by these materials. After 72 h treatment with TMD NSs, no significant mutation of the TA100 bacterial strain was found at various material concentrations, suggesting that the exposure of bacterial cells to these TMDs did not generate genetic mutation and thereby verifying the negligible genotoxicity of 2D MoS₂ and WS₂ NSs.[94]

Bottom-up-synthesized pristine 2D TMDs are generally biocompatible in certain doses. Ultrathin WS₂ NSs produced by hydrothermal treatment of (NH₄)₁₀W₁₂O₄₁·xH₂O and thiourea aqueous solution exhibited negligible *in vitro* cytotoxicity to a human hepatocellular carcinoma cell line (HepG2 cells), a human mammary epithelial cell line (MDA-MB-231 cells) and

a human cervical carcinoma cell line (HeLa cells) with a concentration of no greater than 120 $\mu g\ mL^{-1}$. A further *in vivo* study showed that mice that were intratumorally administered with WS_2 NSs (40 μL, 1.2 mg mL^{-1}) still remained healthy with no obvious body weight and blood parameter variation. This study confirmed the admirable biocompatibility of the bottom-up-synthesized WS_2 NSs both *in vitro* and *in vivo*.[97] In order to broaden the applications of 2D TMDs as nanomedicine, the influences of many crucial parameters such as the size, shape, surface area, types, number of layers and surface groups on their *in vitro* and *in vivo* biocompatibility should be explored.[98] Farokhzad and co-workers found that *n*-BuLi exfoliated MoS_2 NSs could be internalized by cells through three pathways: clathrin → early endosomes → lysosomes, caveolae → early endosomes → lysosomes, and macropinocytosis → late endosomes → lysosomes. MoS_2 NSs could be accumulated in the lysosomes of the cells *via* an autophagy-mediated way and the internalized MoS_2 NSs could be secreted *via* exocytosis and therefore significantly inhibit the exocytosis and reduce the exocytosis-induced MoS_2 NS loss of cancer cells.[99]

A substantial number of findings have evidenced that surface polymer modification plays a crucial role in increasing the biocompatibility of 2D TMD NSs. As such, 2D TMDs with a well-designed surface coating hold promising potential for future translational biomedical applications. Liu *et al.* researched the biocompatibility of double PEGylated MoS_2-IO-(d)PEG NSs using MTT assay and *in vivo* histological analysis. Their findings proved that the viabilities of RAW 264.7 mouse macrophage cells and 4T1 cells were reduced after being treated with MoS_2-IO without PEGylation or MoS_2-IO-single PEG at relatively high MoS_2 concentrations. By contrast, MoS_2-IO-(d)PEG exhibited remarkably reduced toxicity to both cell lines at the same concentration.[100] Not merely MoS_2 NSs, the cytotoxicity of many other kinds of nanomaterials is also closely related to their surface chemistry. It was reported that no significant cytotoxicity of surface-PEGylated *n*-BuLi exfoliated WS_2 NSs was observed for 4T1, HeLa and human embryo kidney (293T) cells when the concentration reached 0.1 mg mL^{-1}. However, WS_2 NSs without PEGylation were toxic to 4T1, HeLa and 293T cells at the same concentration. In another study, Wang and co-workers presented the design of MoS_2–PEG–CpG (cytosine–phosphate–guanine) nanocomposites based on chemically exfoliated MoS_2 NSs.[101] They specified that the intracellular accumulation of CpG could be significantly promoted after the formation of MoS_2-PEG-CpG and the immunotherapeutic effect of CpG could be further enhanced by photothermal treatment. This as-designed MoS_2-PEG-CpG was cyto-compatible with 4T1, RAW 264.7, and HEK293 when the material dose was no more than 50 ppm.

3.1.2 Biodegradation. The biodegradation of 2D TMDs mainly derived from the oxidization of the transition metal element (like $Mo(IV)$ or $W(IV)$) by certain oxidizing agents or the reactive intermediates of certain enzymes. Bianco *et al.* investigated the biodegradability of exfoliated pristine MoS_2 and exfoliated MoS_2 with surface covalent functionalized (f-MoS_2) using plant HRP and human myeloperoxidase (MPO). The biodegradability evaluation using HRP and MPO revealed that the stability of f-MoS_2 NSs is higher than that of pristine MoS_2 sheets in

enzymatic processes.[102] In our group, we studied the *in vitro* biodegradation of Fe(III)@WS_2-PVP nanocapsules in PBS and citrate buffer solution. We found that all the nanocapsules were degraded into NPs after 7 days (Fig. 5a and b). During the degradation period, the light absorbance of the Fe(III)@WS_2-PVP nanocapsules significantly decreased (Fig. 5f) and a transparent colorless solution was formed after 7 days' incubation in PBS (Fig. 5c). Moreover, the degradation is faster in citrate buffer solution and the decrease in the absorbance of Fe(III)@WS_2-PVP in this solution is more distinctive (Fig. 5g). We also studied the chemical nature of the degradation product (7 days in PBS) using XRD (Fig. 5d) and XPS (Fig. 5e), which confirms that the degradation products are composed of Fe_2O_3, $Fe_2(WO_4)_3$ and WO_3. The degradation mechanism can be explained as follows: there exists a redox reaction between Fe(III) and WS_2 to form Fe^{2+} and WO_4^{2-}. The formed Fe^{2+} could be oxidized to Fe^{3+}, which reacts with Fe(III)@WS_2-PVP again to continuously produce Fe^{2+} and WO_4^{2-}. Such a repeated endogenous redox reaction leads to enhanced biodegradation and DOX release of DOX@Fe(III)@WS_2-PVP (Fig. 5h).[103] Liu and co-workers evaluated the biodistribution, excretion, and toxicity of WS_2-PEG, MoS_2-PEG, and TiS_2-PEG *in vivo*, and they concluded that all the nanomaterials showed low toxicity and fast excretion *in vivo*, which paves the way for further biomedical applications. Besides, they reported that TiS_2-PEG and WS_2-PEG continued to exhibit high accumulation levels in the organs for months, while MoS_2-PEG could be degraded and almost completely excreted within 30 days. Such different *in vivo* excretion behaviors could be ascribed to
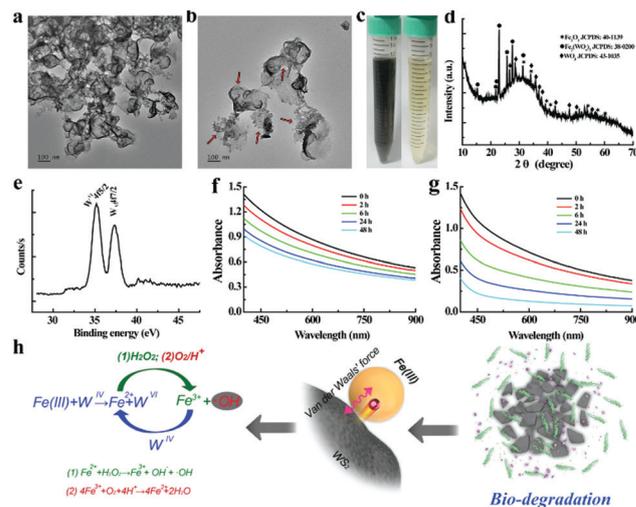

Fig. 5 (a and b) Morphology of Fe(III)@WS_2-PVP nanocapsules (observed using TEM) after being stored in PBS for 72 h (scale bar = 100 nm); (f) time-dependent light absorbance of Fe(III)@WS_2-PVP nanocapsules in PBS; (c) solution images of Fe(III)@WS_2-PVP nanocapsules after being stored in PBS for 0 day (fresh solution: left) and 7 days (right); (g) time-dependent light absorbance of Fe(III)@WS_2-PVP in buffer solution with lower pH; (d) XRD and (e) XPS of 7 day-degradation products in PBS; and (h) enhanced biodegradation and DOX release mechanism of Fe(III)@WS_2-PVP nanocapsules. Yellow balls: Fe(III) species; pink balls: DOX; green lines: PVP. The left picture of panel (h) shows the repeated redox reaction and H_2O_2 and H^+ accelerated the biodegradation process of Fe(III)@WS_2-PVP nanocapsules. Reprinted from ref. 103. Copyright 2017 John Wiley & Sons.

2982 | *J. Mater. Chem. B*, 2020, **8**, 2974–2989

This journal is © The Royal Society of Chemistry 2020

their different chemical properties: TiS_2 is unstable and could be slowly transformed into water-insoluble TiO_2 aggregates and excreted. However, WS_2 is stable under physiological conditions and could hardly be degraded. In sharp contrast, MoS_2 could be oxidized to water-soluble MoO_4^{2-} within the physiological environment and easily excreted *via* both fecal and renal pathways.[104] Notably, bottom-up synthesized 2D TMDs tend to form hierarchical architectures like nanoflowers owing to their high surface area, leading to their enhanced drug-carrying capacity. However, it was reported that the formed MoS_2 nanoflowers exhibited a decreased biodegradability.[105]

3.2   2D TMOs

3.2.1   Biocompatibility. Chen and co-workers researched the *in vitro* cell toxicity of MnO_2-SPs NSs. The viability of cells was determined using the typical CCK-8 assay and it was found that SP-modified 2D MnO_2 nanosheets exhibited low cytotoxicity against 4T1 cells even at a high concentration of 600 μg mL^{-1}. Then, they further studied the biocompatibility of MnO_2-SP NSs by intravenously (I.V.) injecting them into healthy mice at elevated doses (5, 10, and 20 mg kg^{-1}), where no visible damage to major organs of the treated mice was found 30 days post-injection of the NSs.[106]

3.2.2   Biodegradation. Typically, the degradation of 2D TMOs could be initiated under certain environments, owing to the vulnerable chemical properties of central atoms. For example, a novel class of ultrathin 2D SnTe@MnO_2 SP NSs was designed, which showed inherent TME responsive biodegradability. The main metabolite is TeO_3^{2-}, which has a strong antitumor effect. In order to study their biodegradability, PBS and distilled water with different pH values, and GSH or H_2O_2 in distilled water or PBS was employed as the culturing medium. A very slow degradation rate of SnTe NSs in water was confirmed, while in PBS (pH 7.4) the degradation is faster. More strikingly, the addition of H_2O_2, GSH or acid could further increase their degradation. After 24 h of incubation in PBS with H_2O_2, PBS with GSH, or PBS with a pH of 6.5, the original 2D planar structure of the SnTe@MnO_2-SP NSs completely disappeared, and the suspension turned translucent.[107] In another study, Li and co-workers found that PEG-cRGD modified ultra-thin MnO_2 NSs has a pH-dependent degradation ability. By reacting with H_2O_2 in an acidic TME, the MnO_2 NSs could be degraded to Mn(II) ions. After soaking for 10 minutes in PBS (pH = 5) containing H_2O_2, the degradation was more evident and could be demonstrated by the change in shape and structural collapse within the first 60 min. Since cancer cells usually have high H_2O_2 levels and low pH, the biodegradability of such nanoflakes will facilitate their use in cancer therapy.[43] MoOx@F127 NSs exhibit significant degradation behavior at different pH values, which could degrade rapidly in alkaline solutions, while they are very stable in acidic solutions (Fig. 6a and b: the decrease of light absorbance means the degradation of MoOx@F127 NSs). MoOx@F127 NSs maintained their structural integrity at pH 5.4 (Fig. 6c), but underwent obvious structure destruction (Fig. 6d) when cultured at a pH value of 7.4. In marked contrast, MoOx@F127 NSs transformed into particles with an ultra-small
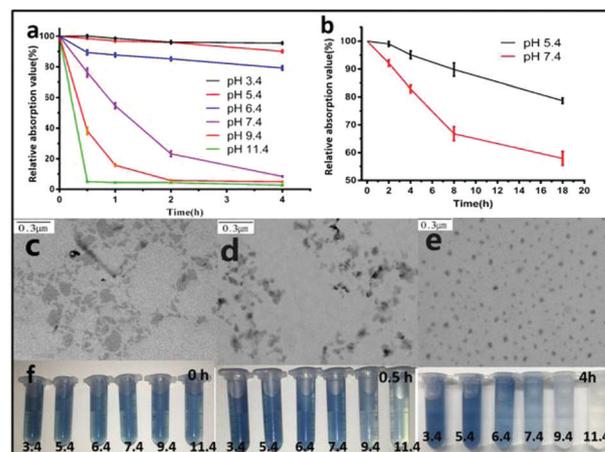

Fig. 6 The decrease of the relative absorption value of MoOx@F127 NSs during the degradation process in (a) PBS or (b) 40% serum solution with pH; (c–e) morphologies of 2 h degraded MoOx@F127 NSs in PBS at pH (c) 5.4, (d) 7.4 and (e) 11.4, observed by TEM; and (f) solutions of MoOx@F127 NSs in PBS with different pHs for 0 h, 0.5 h, and 4 h. Reprinted from ref. 45. Copyright 2019 Elsevier B.V.

diameter and their sheet-like morphology could not be observed at pH 11.4 (2 h, Fig. 6e). The solution color also showed pH- and time-dependent fading (Fig. 6f). The degradation is mainly caused by the oxidation of Mo^V to Mo^{VI}, while the pH-enhanced degradation may be due to the different oxidation rates.[45]

3.3   2D BPs

3.3.1   Biocompatibility. 2D BPs feature superior surface activity, tunable bandgaps, excellent biodegradability, and good biocompatibility. Although BPs could be prepared *via* acoustic-microfluidic stripping, solvothermal treatment, electrochemical exfoliation, liquid-phase ultrasonic exfoliation, mechanical cleavage, *etc.*, how to tune their bio-degradability remains a great challenge. Qu *et al.* discovered that BP NSs with titanium sulfonate ligand coating did not show any obvious adverse inflammatory responses.[108] Using a high energy mechanical milling approach or the oil-in-water emulsion solvent evaporation method, BP was successfully coordinated with polylactic-*co*-glycolic acid or polyethylene glycol.[109] The *in vitro* biocompatibility of PEGylated flake-shaped BP-Au NP nanohybrids was studied using MTT assay, which suggested no obvious toxic effects on HeLa, HepG2, and 4T1 cells even if their concentration is as high as 128 μg mL^{-1}.[110] However, *in vitro* research found that BP NSs with a concentration of 200 μg mL^{-1} could induce apoptosis of HeLa cells. Moreover, it was uncovered that BP NSs could induce transient oxidative stress including DNA double-stranded breaks, reduction of catalase activity, lysosomal swelling, lipid peroxidation, mitochondrial ROS production, and bone marrow nucleated cell damage. Fortunately, this could be gradually recovered to normal levels and will not cause pathological issues to major internal organs like liver, spleen, *etc.*[111] Raucci *et al.* pointed out that pristine 2D BP could inhibit the metabolic activity of osteosarcoma cells while supporting both the proliferation and osteogenic differentiation of

mesenchymal stem cells and human preosteoblast cells. Moreover, it was found that 2D BP could increase the generation of anti-inflammatory cytokines and thus inhibit the synthesis of pro-inflammatory mediators, suggesting the chance of preventing cancer-related inflammation.[112] BP at certain concentration can penetrate the cell membrane, by generating intracellular reactive oxygen species (ROS).[113] For example, Lim and co-workers investigated the cytotoxic effects of layered BP on both cell metabolic activity and membrane integrity against L929 cells. Their findings indicate that BP at concentrations lower than 4 μg mL^{-1} can lead to cell cytotoxicity by oxidative stress-mediated enzyme activity reduction and membrane disruption.[114]

3.3.2 Biodegradation. Within a living organism, BP NSs could react with water and oxygen and transform into non-toxic degradation products, leading to the biodegradation of BP nanosheets. As a representative report, the unique biodegradability of BPQD/PLGA NSs was indicated, which will be degraded to nontoxic phosphate and phosphonate and eventually cleared out from the body. The potential degradation could be explained by the fact that the external PLGA shells of the BPQD/PLGA NSs will be degraded gradually into segments, oligomers and monomers owing to the hydrolysis of the ester linkage in the physiological environment.[115] By using Raman scattering mapping, the degradation behavior of BPs in different cells was studied. It was found that a flaky BP nanomaterial prepared by a liquid-phase ultrasonic exfoliation method exhibits good biodegradation.[116] Besides, the degradation degrees of BPs were different in normal and tumor cells owing to their different microenvironments. Moreover, the preferable degradation in tumor cells could inhibit their proliferation by increasing the concentration of intracellular phosphate anions, but will not cause an obvious adverse effect on normal cells. Different cell lines (A549, MCF-7 and (human bone mesenchymal stem cells) hBMSCs) were incubated with BPs (4 μg mL^{-1}). After being homogenized for various time periods, the Raman intensities of the cells were monitored, and the total characteristic peak areas were recorded to reflect the intracellular degradation degree of BP. As can be found in Fig. 7a, the decrease of the intracellular Raman intensity of hBMSCs is less obvious. Specifically, a significantly enhanced Raman intensity could be observed for MCF-7 and A549 cancerous cells, indicating a fast intracellular degradation of BP in these cells. Meanwhile, compared with hBMSCs, these cancer cells exhibited a BP-degradation dependent sharp increase of the intracellular phosphate concentration (Fig. 7b). Besides the degradation, the time- and dosage-dependent and cancer-cell-selective inhibition of cell proliferation was further observed (Fig. 7c and d). The IC50 values for HeLa, A549, and MCF-7 cells are lower than 2 μg mL^{-1} (at 48 h); however, good cell viability is verified for hBMSCs and QSG-7701 cells.

3.4 2D MOFs

3.4.1 Biocompatibility. MOFs have been used for drug delivery and tumor therapy, as they have the merits of small size, high drug loadings, versatile functionality, and distinct biodegradability owing to their labile metal–ligand bonds. HT-29 human colon adenocarcinoma cells were used to verify
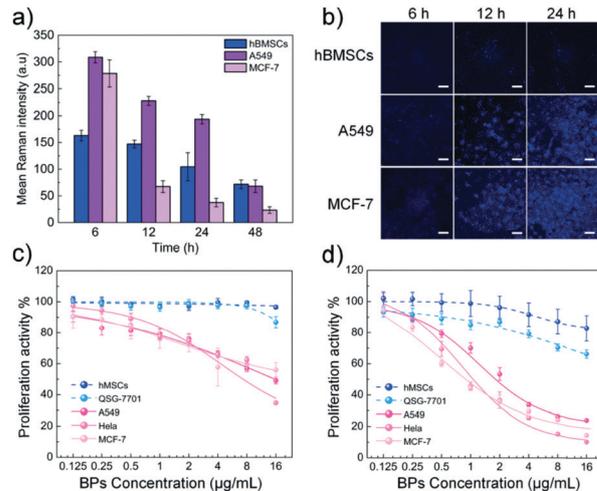

Fig. 7 (a) Raman scattering mapping indicated the intracellular degradation of BPs (the y-axis was plotted by determining the total areas of A_{1g}, B_{2g}, and A_{2g} peaks); (b) intracellular phosphate anion concentrations of cells treated with BPs for different time durations (determined by the phosphate fluorescent probe); and (c and d) dose-dependent cell activities of different cell lines after treatment with BPs for (c) 24 h and (d) 48 h ($n = 4$). Reprinted with permission from ref. 116. Copyright 2019 John Wiley & Sons.

the cytotoxicity of Tb-MOF by selecting c,c,t-(diamminedichloro-disuccinato) Pt(IV) and Tb^{3+} ions as the ligand and central atoms, respectively. It was found that the particles undergo receptor-mediated endocytosis and could then be decomposed through an intracellular reduction environment.[117] Liu et $al.$ synthesized Zn-TCPP@PEG/DOX NSs for chemo-photodynamic cancer therapy. In their study, Zn-TCPP@PEG/DOX NSs caused no detectable toxicity to the studied cell-lines without being exposed to light. The levels of Zn^{2+} in different organs of mice were measured by ICP-OES after Zn-TCPP@PEG injection. Most of the Zn^{2+} ions were found to be excreted after one week, which indicated that the MOFs could be effectively removed from the body of the mice.[61] Qu et $al.$ proved that top-down exfoliated ultrasmall porphyrinic MOF QDs using an ultrasonic route (Fig. 8a and b) could produce ROS twice as effectively as porphyrinic nano-MOFs. MTT assays showed that the viability of HeLa cells was
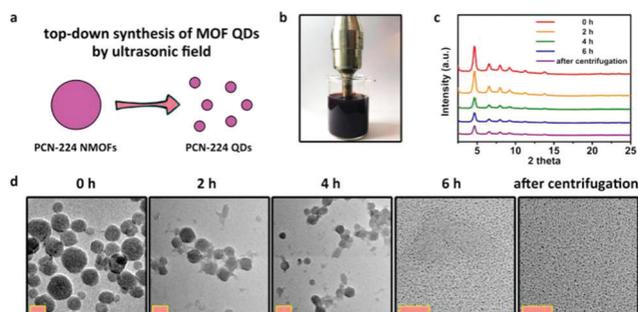

Fig. 8 (a) Scheme of the ultrasound-assisted top-down synthesis of PCN-224 QDs; (b) photo of the correlated ultrasonic process; (c and d) time-dependent (c) XRD patterns and (d) TEM images of porphyrinic nano-MOFs after ultrasonic treatment for different time durations. Scale bar = 50 nm. Reprinted from ref. 118. Copyright 2019 American Chemical Society.

2984 | J. Mater. Chem. B, 2020, **8**, 2974–2989

This journal is © The Royal Society of Chemistry 2020

not affected by such MOF QD. Besides, the as-prepared MOF QDs could be effectively absorbed by HeLa cells. It was found that the top-down synthesized MOF QDs showed low toxicity and could be excreted mainly through the renal pathway, mainly owing to the ultrasonic time-dependent decreased size of the products (Fig. 8d). However, the ultrasound did not alter their crystallinity even after receiving a 6 h ultrasound treatment (Fig. 8c).[118]

3.4.2 Biodegradation. In recent years, 2D MOFs have been frequently used in the field of biomedicine as a novel class of 2D biodegradable NSs. The degradation of 2D MOFs can also be derived from the oxidization of central metal atoms. For example, a core–shell MOF (Fe$_3$O$_4$@C@MIL-100(Fe)) was fabricated in order to deliver dihydroartemisinin (DHA) and Fe(III) to tumor sites. It was reported that MOFs could decompose their structure in different environments such as a tumor acidic microenvironment and high temperature. When the substance reaches the tumor site, Fe(III) is reduced to Fe(II) in an acidic environment, inducing the destruction of the MOF structure, and Fe(II) reacts with DHA, which is released in an acidic environment to produce cytotoxic ROS. Besides, the magnetic core of Fe$_3$O$_4$@C endows it with MRI capability. Moreover, the degradation of outer MIL-100(Fe) increases (MIL = Materials of Institute Lavoisier) with a decrease of the pH value of PBS. As outer MIL-100(Fe) continuously degraded, the release of iron ions increased.[119]

3.5 2D B and BN

3.5.1 Biocompatibility. BN NSs and BN NS based composites have been frequently designed as nano-platforms for biomedical applications.[65,66,120] 2D BN NSs prepared by delaminating solvent-free mechano-chemically exfoliated bulk h-BNs do not show detectable cytotoxicity to normal cells. After loading with DOX, the tumor cells' inhibition effectiveness of the DOX did not change.[69] Poly-diallyldimethylammonium chloride (PDDA) stabilized PDDA-BN-GNC (gold nanocluster composite) multifunctional composites also showed excellent biocompatibility and the cell viability was greater than 90% after 48 h incubation with a high material concentration of 100 μg mL^{-1}.[66] The cytotoxicity of hexagonal boron nitride NS/graphene quantum dot (hBN–GQD) nanocomposites was evaluated using MTT assay. Due to the facts that GQDs are a low toxicity carbon material and BN materials are biocompatible with cells, the cell viability still remained at 93.2% and 84.3% after interacting with hBN–GQDs (200 μg mL^{-1}) for 24 h and 48 h, respectively.[65]

3.5.2 Biodegradation. The degradation of 2D B NSs has not been studied yet until now, while BN NSs will experience a disintegration either by wet-oxidation or under the action of enzymes. To simultaneously achieve the desired biodegradation and high therapeutic efficacy, coupling BN NSs with certain surface functional materials is always necessary. For example, Zeng et al. reported that the incorporation of BN NSs with biocompatible CS could make the resultant BN-CS NSs more biocompatible.[120] Moreover, crystallinity may also influence the degradation rate of a certain substance. For example, Luan and co-workers discussed the degradation mechanisms of SiC(f)/BN(i)/[SiC-B$_4$C](m) under different oxidizing conditions (oxygen and wet (8% O$_2$:12% H$_2$O:80% Ar) and oxygen and

dry (99.99% Ar:0.01% O$_2$)). This study found that the oxidant content could affect the degradation of the composite. Under a wet oxygen atmosphere, the B$_4$C layers and the SiC matrix underwent severe oxidation, which could protect the SiC fiber and the BN interphase by sealing the matrix cracks with borosilicate. However, under the dry oxygen atmosphere, both the B$_4$C and BN interphase layers were consumed and disappeared only in part owing to the insufficient oxygen supply and the high volatilization rate.[121] Bianco et al. reported the biodegradability of hBN NSs using HRP and MPO with the photo-Fenton reaction. The results showed that hBN NSs treated with MPO underwent significant degradation, while the effect of HRP on hBN is not obvious (not observed within 60 days). Interestingly, the photo-Fenton reaction caused an almost complete degradation within 100 h, suggesting that extensive oxidation of hBN NSs needs much more powerful oxidants, such as hydroxyl radicals.[122] Recently, the biodegradation of h-BNs was studied in lysosome mimicking solution and PBS for oxidative degradation and hydrolytic degradation, respectively. The conclusions indicated that hBN-colemanite with high crystallinity is resistant to both hydrolytic and oxidative degradation, while hBN-boric acid and hBN-boron trioxide are more prone to degradation in both lysosome mimicking solution and PBS.[123]

3.6 2D LDHs

MTT and CCK-8 assays are two powerful methods that are frequently used in the in vitro biocompatibility evaluation of nanomaterials. Beyond them, other protocols could also be used for cell viability detection. For example, Gu et al. reported the use of alamarBlue assay to study the cyto-compatibility of PEG/Fe-LDHs in vitro (in Hs27 fibroblast cells). The results suggested that the in-cell viability after 24 h incubation of PEG/Fe-LDHs showed no obvious reduction at pH 7.4, and the upper limit of tolerance in vitro was 12 μg mL^{-1}. Then, typical in vivo biosafety assay methods like body weight monitoring, blood safety, and histo-compatibility evaluations were performed to study their in vivo biocompatibility, and these data collectively revealed that the upper limit of tolerance is 100 mg kg^{-1} Fe for mice.

Such 2D LDHs are also degradable owing to their special physicochemical properties, or external stimuli. Real-time TEM after immersing them in acid buffer indicates the decomposition of the NS edges in the initial 10–30 min. With the extension of the incubation time, the entire NSs collapsed. They believed that such a "center-to-edge" disintegration behavior of Fe–Al LDH could be ascribed to the surface PEGylation. Meanwhile, H$^+$ ions could easily penetrate into the interlayer gallery and then protonate the central OH groups. Obvious particles still could be observed after 4 h, further implying the NS edge disintegration and the complete collapse of NSs. Such a biodegradable behavior of PEG/Fe-LDHs is anticipated to facilitate their Fenton reaction activity and contributes to their biocompatibility as a biomedically applicable nanomaterial.[73]

3.7 2D metals

Notably, special attention should be paid to the cytotoxicity of 2D metal NSs since they are likely to be corrosive to release

certain amounts of metal ions. In an earlier study, Zheng and co-workers investigated the influence of surface coatings on the biocompatibility and behaviors including the biodistribution, the half-life time in blood circulation, the potential toxicity to organs, and the clearance route of Pd NSs in mice. The MTT assays proved that the HeLa cells' viability remained greater than 85% when incubated with different modified Pd NSs with a concentration of 150 μg mL^{-1} for 1 day, indicating that the different surface modifications could endow Pd NSs with admirable cyto-compatibility. Compared with several biocompatible molecules like PEG-NH$_2$, carboxymethyl chitosan, and dihydrolipoic acid-zwitterions, Pd NSs modified with PEG-SH were proved to have an ultra-long blood circulation half-life and showed high uptake in tumors.[111] Zeng evaluated the biosafety of MnPc@HA NSs from the viewpoints of hemolysis and cytotoxicity assays. After 8 h incubation with MnPc@HA NSs, red blood cells showed no noticeable hemolysis. The *in vivo* biocompatibility assessment was performed by I.V. injecting the MnPc@HA NSs into the mice. The blood biochemistry analysis reveals that all blood cell numbers are in the normal ranges. The collected biochemistry parameters that could reflect the liver and kidney functions remained almost the same as those of healthy mice, suggesting the admirable hemo-compatibility of MnPc@HA NSs. To evaluate their cyto-compatibility, 4T1, L929, and HeLa cells were, respectively, incubated with MnPc@HA NSs, and it was found that their viabilities all remained higher than 90% at a material dose of 100 μg mL^{-1}.[124]

Until now, very little has been studied about the biodegradation possibilities of 2D metal NSs; however, one could look for the breakthrough from the biodegradation of metal-based bulk biomaterials. Moreover, it is worth mentioning that special attention needs to be paid to the *in vivo* metal degradation induced biological consequences. Taking total hip arthroplasty as an example, the *in vivo* local biological consequences to metal degradation include mild asymptomatic tissue damage and severe soft tissue and bone destruction. Such severe soft tissues and bone lesions are deemed as adverse reactions to aseptic lymphocytic vasculitis associated pseudotumors, lesions, and metal debris. Moreover, metal particle dissemination and degraded ions could also arouse many systemic adverse effects such as cancerogenesis, organ toxicity, teratogenicity, and immunotoxicity in the body.[125]

3.8 Other 2D nanomaterials

The potential *in vitro* toxicity of Ti$_3$C$_2$-SP to cells was tested by a CCK-8 assay. After incubating 4T1 cells with Ti$_3$C$_2$-SP at varying concentrations for 1 and 2 days, a negligible side effect on the survival of 4T1 cells was found, although further confocal laser scanning microscopy images showed that Ti$_3$C$_2$-SP NSs were efficiently taken up by these cells. A further *in vivo* biocompatibility test also showed no detectable pathological toxicity.[90] Recently, Shi and co-workers studied the degradation of silicene nanosheets (SNSs), by dispersing the as-prepared SNSs in water and in air at room temperature. The changes in the chemical structure, light absorption, and morphology of SNSs during 14 days' storage were analyzed. As time went by, the dark appearance of the SNS suspension gradually faded and turned out to be transparent

after 14 days. After being stored in water and air for 3 days, small visible NPs could be found on the surfaces, indicating the happening of the surface oxidation of SNSs in water. Furthermore, the degradation was found to be more evident and the SNSs' morphology substantially changed after 7 days and was destroyed with very few sheet-like objects left after 14 days. The chemical nature study of the degradation product found the existence of SiO–OH$_x$ (–OOH terminated), SiO$_x$ (–O terminated), and Si–OH (–OH terminated). MD simulations were performed, which showed that only water molecules could not destroy the structural integrity of SNSs and therefore the entire degradation could be explained as the mechanism of 3($\equiv$Si–) + O$_2$ + H$_2$O → –SiO– + –Si–OH + $\equiv$Si– + OH– → –SiO– + 2(–SiOH–).[89]

4. Conclusions and outlook

Although the existing 2D nanomaterials have shown some tentative and encouraging *in vitro* and *in vivo* biocompatibility, there is still much room for improvement of these 2D nanoplatforms for tumor theranostics. The engineering of a new generation of intelligent, biocompatible and multifunctional nanostructures that could integrate multiple functionalities of various materials to obtain an "all-in-one" platform is also a potential starting point for translational research. In addition, it is worth noting that although the literature reported the relatively low-to-negligible toxicity of various kinds of 2D nanomaterials at cell and animal levels, there is still a long distance to go to reach a consensus about the safe concentration of every 2D nanomaterial. This may be due to the differences in the materials' preparation methods, cell lines, and other experimental conditions.

Considering the *in vivo* biodistribution of 2D nanomaterials, more systematic studies are necessary to know about the detailed metabolism of 2D materials in longer terms. Kim and co-workers studied for the first time the effects of MoS$_2$, WS$_2$, and BN nanosheets on human adipose-derived mesenchymal stem cells (hADMSCs). After coating them on cell-culture substrates by a drop-casting method, no acute toxicity was observed with any of the 2D materials over a low concentration range (less than 5 mg mL^{-1}). Interestingly, it was found that the MoS$_2$, WS$_2$, and BN nanosheet modified substrates can promote the adhesion, spreading, proliferation and adipogenic differentiation of hADMSCs. Therefore, 2D materials could act as favorable substrates to control stem cell growth and differentiation, which might be highly advantageous in both biomedical research and therapy.[126] However, much research on the influence of various 2D nanosheets on the viability of stem cells and other cell lines except for cancer cells is still needed. The surfaces of 2D materials could be finely tuned *via* various surface chemical modifications; however, during the process of the *in vivo* applications of 2D nanomaterials, the amount of administered (usually I.V. injection) 2D NSs that could reach the targeted locations was still limited. A large amount of injected 2D materials will be circulated in blood and captured by RES organs, which will inevitably bring possible safety threats to tissue.[27] On this ground, more active tumor-targeting ligands that could modify 2D nanosystems may improve

2986 | *J. Mater. Chem. B*, 2020, **8**, 2974–2989

This journal is © The Royal Society of Chemistry 2020

their therapeutic efficacy. In general, although the applied research studies of 2D materials are now on a laboratory-scale and still at their early stage, the design, synthesis and biodegradation research studies of 2D materials are the much-focused frontier in the domains of materials science, nanobiotechnology, and nanomedicine.

Conflicts of interest

There are no conflicts to declare.

Acknowledgements

Notes and references

1 S. G. Wang, L. L. Zhou, Y. T. Zheng, L. N. Li, C. Y. Wu, H. L. Yang, M. X. Huang and X. An, *Colloids Surf., A*, 2019, **583**, 124004.

2 Y. Yang, A. M. Asiri, Z. Tang, D. Du and Y. Lin, *Mater. Today*, 2013, **16**, 365–373.

3 P. Bollella, G. Fusco, C. Tortolini, G. Sanzo, G. Favero, L. Gorton and R. Antiochia, *Biosens. Bioelectron.*, 2017, **89**, 152–166.

4 H. Q. Bao, Y. Z. Pan, Y. Ping, N. G. Sahoo, T. F. Wu, L. Li, J. Li and L. H. Gan, *Small*, 2011, **7**, 1569–1578.

5 H. Zhang, H. Wu, J. Wang, Y. Yang, D. Wu, Y. Zhang, Y. Zhang, Z. Zhou and S. Yang, *Biomaterials*, 2015, **42**, 66–77.

6 H. Lin, Y. Chen and J. Shi, *Adv. Sci.*, 2018, **5**, 1800518.

7 Y. Chen, C. Tan, H. Zhang and L. Wang, *Chem. Soc. Rev.*, 2015, **44**, 2681–2701.

8 X. Huang, Z. Y. Zeng and H. Zhang, *Chem. Soc. Rev.*, 2013, **42**, 1934–1946.

9 M. Chhowalla, Z. Liu and H. Zhang, *Chem. Soc. Rev.*, 2015, **44**, 2584–2586.

10 P. Joensen, R. Frindt and S. R. Morrison, *Mater. Res. Bull.*, 1986, **21**, 457–461.

11 C. Tan, P. Yu, Y. Hu, J. Chen, Y. Huang, Y. Cai, Z. Luo, B. Li, Q. Lu and L. Wang, *J. Am. Chem. Soc.*, 2015, **137**, 10430–10436.

12 S. S. Chou, B. Kaehr, J. Kim, B. M. Foley, M. De, P. E. Hopkins, J. Huang, C. J. Brinker and V. P. Dravid, *Angew. Chem., Int. Ed.*, 2013, **125**, 4254–4258.

13 T. Liu, C. Wang, W. Cui, H. Gong, C. Liang, X. Shi, Z. Li, B. Sun and Z. Liu, *Nanoscale*, 2014, **6**, 11219–11225.

14 T. Liu, C. Wang, X. Gu, H. Gong, L. Cheng, X. Shi, L. Feng, B. Sun and Z. Liu, *Adv. Mater.*, 2014, **26**, 3433–3440.

15 W. Yin, L. Yan, J. Yu, G. Tian, L. Zhou, X. Zheng, X. Zhang, Y. Yong, J. Li and Z. Gu, *ACS Nano*, 2014, **8**, 6922–6933.

16 G. Eda, H. Yamaguchi, D. Voiry, T. Fujita, M. Chen and M. Chhowalla, *Nano Lett.*, 2011, **11**, 5111–5116.

17 Y. Yu, L. Teng, C. Liang, G. Song, L. Zhuang and M. Chen, *ACS Appl. Mater. Interfaces*, 2015, **7**, 7526–7533.

18 C. Zhu, Z. Zeng, H. Li, F. Li, C. Fan and H. Zhang, *J. Am. Chem. Soc.*, 2013, **135**, 5998–6001.

19 C. Tan, X. Qi, X. Huang, J. Yang, B. Zheng, Z. An, R. Chen, J. Wei, B. Z. Tang and W. Huang, *Adv. Mater.*, 2014, **26**, 1735–1739.

20 Y. Zhang, B. Zheng, C. Zhu, X. Zhang, C. Tan, H. Li, B. Chen, J. Yang, J. Chen and Y. Huang, *Adv. Mater.*, 2015, **27**, 935–939.

21 J. E. Kim, D. Yim, C. H. Lee, B. Jun, J. Nam, S. H. Han, S. U. Lee, J.-H. Kim and J. W. Kim, *Adv. Funct. Mater.*, 2018, **28**, 1802737.

22 J. Guo, Y. Cao, R. Shi, G. I. N. Waterhouse, L.-Z. Wu, C.-H. Tung and T. Zhang, *Angew. Chem., Int. Ed.*, 2019, **58**, 8443–8447.

23 S. Su, W. Cao, W. Liu, Z. Lu, D. Zhu, J. Chao, L. Weng, L. Wang, C. Fan and L. Wang, *Biosens. Bioelectron.*, 2017, **94**, 552–559.

24 Y. Y. Liu, Y. X. Xi, J. L. Zhao, J. Y. Zhao, J. C. Li, G. Q. Huang, J. Q. Li, F. Fang, L. L. Gu and S. G. Wang, *Chem. Eng. J.*, 2019, **375**, 122048.

25 Y. T. Zheng, W. F. Wang, J. L. Zhao, C. Y. Wu, C. Q. Ye, M. X. Huang and S. G. Wang, *Carbohydr. Polym.*, 2019, **222**, 115039.

26 Y. Yong, L. Zhou, Z. Gu, L. Yan, G. Tian, X. Zheng, X. Liu, X. Zhang, J. Shi, W. Cong, W. Yin and Y. Zhao, *Nanoscale*, 2014, **6**, 10394–10403.

27 S. Wang, K. Li, Y. Chen, H. Chen, M. Ma, J. Feng, Q. Zhao and J. Shi, *Biomaterials*, 2015, **39**, 206–217.

28 X. Ding, F. Peng, J. Zhou, W. Gong, G. Slaven, K. P. Loh, C. T. Lim and D. T. Leong, *Nat. Commun.*, 2019, **10**, 41.

29 Z. Zeng, Z. Yin, X. Huang, H. Li, Q. He, G. Lu, F. Boey and H. Zhang, *Angew. Chem., Int. Ed.*, 2011, **50**, 11093–11097.

30 Z. Zeng, T. Sun, J. Zhu, X. Huang, Z. Yin, G. Lu, Z. Fan, Q. Yan, H. H. Hng and H. Zhang, *Angew. Chem., Int. Ed.*, 2012, **51**, 9052–9056.

31 K. Yang, G. Yang, L. Chen, L. Cheng, L. Wang, C. Ge and Z. Liu, *Biomaterials*, 2015, **38**, 1–9.

32 W. Feng, W. Nie, Y. Cheng, X. Zhou, L. Chen, K. Qiu, Z. Chen, M. Zhu and C. He, *Nanomedicine*, 2015, **11**, 901–912.

33 X. Qian, S. Shen, T. Liu, L. Cheng and Z. Liu, *Nanoscale*, 2015, **7**, 6380–6387.

34 L. Cheng, S. Shen, S. Shi, Y. Yi, X. Wang, G. Song, K. Yang, G. Liu, T. E. Barnhart and W. Cai, *Adv. Funct. Mater.*, 2016, **26**, 2185–2197.

35 L. Cheng, C. Yuan, S. D. Shen, X. Yi, H. Gong, K. Yang and Z. Liu, *ACS Nano*, 2015, **9**, 11090–11101.

36 K. Kalantar-zadeh, J. Z. Ou, T. Daeneke, A. Mitchell, T. Sasaki and M. S. Fuhrer, *Appl. Mater. Today*, 2016, **5**, 73–89.

37 D. Chimene, D. L. Alge and A. K. Gaharwar, *Adv. Mater.*, 2015, **27**, 314–316.

38 Y. Chen, D. Ye, M. Wu, H. Chen, L. Zhang, J. Shi and L. Wang, *Adv. Mater.*, 2014, **26**, 7018.

This journal is © The Royal Society of Chemistry 2020

J. Mater. Chem. B, 2020, **8**, 2974–2989 | **2987**

39 S. Kim, S. M. Ahn, J. S. Lee, T. S. Kim and D. H. Min, *2D Mater.*, 2017, **4**, 025069.

40 Y. Yuan, S. Wu, F. Shu and Z. Liu, *Chem. Commun.*, 2014, **50**, 1095–1097.

41 W. Tang, W. Fan, W. Zhang, Z. Yang, L. Li, Z. Wang, Y.-L. Chiang, Y. Liu, L. Deng, L. He, Z. Shen, O. Jacobson, M. A. Aronova, A. Jin, J. Xie and X. Chen, *Adv. Mater.*, 2019, **31**, 1900401.

42 X.-L. Hu, Q. Ca, J. Gao, R. A. Field, G.-R. Chen, N. Jia, Y. Zang, J. Li and X.-P. He, *ACS Appl. Mater. Interfaces*, 2019, **11**, 22181–22187.

43 D. W. Zeng, L. Wang, L. Tian, S. L. Zhao, X. F. Zhang and H. Y. Li, *Drug Delivery*, 2019, **26**, 661–672.

44 G. Song, J. Hao, C. Liang, T. Liu, M. Gao, L. Cheng, J. Hu and Z. Liu, *Angew. Chem., Int. Ed.*, 2015, **55**, 2122–2126.

45 Y. J. Chen, A. R. Khan, D. X. Yu, Y. J. Zhai, J. B. Ji, Y. K. Shi and G. X. Zhai, *J. Colloid Interface Sci.*, 2019, **553**, 567–580.

46 K. Vimala, K. Shanthi, S. Sundarraj and S. Kannan, *J. Colloid Interface Sci.*, 2016, **488**, 92–108.

47 M. Luo, T. Fan, Y. Zhou, H. Zhang and L. Mei, *Adv. Funct. Mater.*, 2019, **29**, 1808306.

48 Z. B. Sun, H. H. Xie, S. Y. Tang, X. F. Yu, Z. N. Guo, J. D. Shao, H. Zhang, H. Huang, H. Y. Wang and P. K. Chu, *Angew. Chem., Int. Ed.*, 2015, **54**, 11526–11530.

49 S. Anju, J. Ashtami and P. V. Mohanan, *Mater. Sci. Eng., C*, 2019, **97**, 978–993.

50 X. Zeng, M. Luo, G. Liu, X. Wang, W. Tao, Y. Lin, X. Ji, L. Nie and L. Mei, *Adv. Sci.*, 2018, **5**, 1800510.

51 H. Fu, Z. Li, H. Xie, Z. Sun, B. Wang, H. Huang, G. Han, H. Wang, P. K. Chu and X.-F. Yu, *RSC Adv.*, 2017, **7**, 14618–14624.

52 W. Tao, X. Zhu, X. Yu, X. Zeng, Q. Xiao, X. Zhang, X. Ji, X. Wang, J. Shi and H. Zhang, *Adv. Mater.*, 2017, **29**, 1603276.

53 X. Wang, J. Shao, M. Abd El Raouf, H. Xie, H. Huang, H. Wang, P. K. Chu, X.-F. Yu, Y. Yang, A. M. AbdEl-Aal, N. H. M. Mekkawy, R. J. Miron and Y. Zhang, *Biomaterials*, 2018, **179**, 164–174.

54 M. Qiu, D. Wang, W. Liang, L. Liu, Y. Zhang, X. Chen, D. K. Sang, C. Xing, Z. Li, B. Dong, F. Xing, D. Fan, S. Bao, H. Zhang and Y. Cao, *Proc. Natl. Acad. Sci. U. S. A.*, 2018, **115**, 501–506.

55 H. Cheng, Y. Liu, Y. Hu, Y. Ding, S. Lin, W. Cao, Q. Wang, J. Wu, F. Muhammad, X. Zhao, D. Zhao, Z. Li, H. Xing and H. Wei, *Anal. Chem.*, 2017, **89**, 11552–11559.

56 M. Zhao, Q. Lu, Q. Ma and H. Zhang, *Small Methods*, 2017, **1**, 1600030.

57 M. Zhao, Y. Wang, Q. Ma, Y. Huang, X. Zhang, J. Ping, Z. Zhang, Q. Lu, Y. Yu and H. Xu, *Adv. Mater.*, 2015, **27**, 7372–7378.

58 Y. Wang, M. Zhao, J. Ping, B. Chen, X. Cao, Y. Huang, C. Tan, Q. Ma, S. Wu, Y. Yu, Q. Lu, J. Chen, W. Zhao, Y. Ying and H. Zhang, *Adv. Mater.*, 2016, **28**, 4149–4155.

59 M. Xu, S. Yuan, X.-Y. Chen, Y.-J. Chang, G. S. Day, Z.-Y. Gu and H.-C. Zhou, *J. Am. Chem. Soc.*, 2017, **139**, 8312–8319.

60 X. Gao, R. Cui, M. Zhang and Z. Liu, *Mater. Lett.*, 2017, **197**, 217–220.

61 W. Zhu, Y. Yang, Q. Jin, Y. Chao, L. Tian, J. Liu, Z. Dong and Z. Liu, *Nano Res.*, 2019, **12**, 1307–1312.

62 X. Ji, N. Kong, J. Wang, W. Li, Y. Xiao, S. T. Gan, Y. Zhang, Y. Li, X. Song and Q. Xiong, *Adv. Mater.*, 2018, **30**, 1803031.

63 H. Zeng, C. Zhi, Z. Zhang, X. Wei, X. Wang, W. Guo, Y. Bando and D. Golberg, *Nano Lett.*, 2010, **10**, 5049–5055.

64 Y. Lin and J. W. Connell, *Nanoscale*, 2012, **4**, 6908–6939.

65 J. Peng, S. Wang, P.-H. Zhang, L.-P. Jiang, J.-J. Shi and J.-J. Zhu, *J. Biomed. Nanotechnol.*, 2013, **9**, 1679–1685.

66 G.-H. Yang, J.-J. Shi, S. Wang, W.-W. Xiong, L.-P. Jiang, C. Burda and J.-J. Zhu, *Chem. Commun.*, 2013, **49**, 10757–10759.

67 G.-H. Yang, A. Abulizi and J.-J. Zhu, *Ultrason. Sonochem.*, 2014, **21**, 1958–1963.

68 V. Kumar, D. Lahiri and I. Lahiri, *Mater. Today: Proc.*, 2018, **5**, 16756–16762.

69 O. P. Gnatyuk, G. I. Dovbeshko, A. Yershov, S. O. Karakhim, O. Ilchenko and O. Y. Posudievsky, *RSC Adv.*, 2018, **8**, 30404–30411.

70 K. Ladewig, Z. P. Xu and G. Q. Lu, *Expert Opin. Drug Delivery*, 2009, **6**, 907–922.

71 F. Mi, X. Chen, Y. Ma, S. Yin, F. Yuan and H. Zhang, *Chem. Commun.*, 2011, **47**, 12804–12806.

72 F. L. Theiss, G. A. Ayoko and R. L. Frost, *Appl. Surf. Sci.*, 2016, **383**, 200–213.

73 Z. Cao, L. Zhang, K. Liang, S. Cheong, C. Boyer, J. J. Gooding, Y. Chen and Z. Gu, *Adv. Sci.*, 2018, **5**, 201801155.

74 L. J. Wang, H. Y. Xing, S. J. Zhang, Q. G. Ren, L. M. Pan, K. Zhang, W. B. Bu, X. P. Zheng, L. P. Zhou, W. J. Peng, Y. Q. Hua and J. L. Shi, *Biomaterials*, 2013, **34**, 3390–3401.

75 J. M. Oh, S. J. Choi, G. E. Lee, S. H. Han and J. H. Choy, *Adv. Funct. Mater.*, 2009, **19**, 1617–1624.

76 A. Hanif, M. Sun, S. Shang, Y. Tian, A. C. K. Yip, Y. S. Ok, I. K. M. Yu, D. C. W. Tsang, Q. Gu and J. Shang, *J. Hazard. Mater.*, 2019, **374**, 365–371.

77 Z. Guo, M. Chen, C. Peng, S. Mo, C. Shi, G. Fu, X. Wen, R. Zhuang, X. Su and T. Liu, *Biomaterials*, 2018, **179**, 134.

78 Y. Huang, X. Chen, S. Shi, M. Chen, S. Tang, S. Mo, J. Wei and N. Zheng, *Sci. China: Chem.*, 2015, **58**, 1753–1758.

79 Z. Zhao, S. Shi, Y. Huang, S. Tang and X. Chen, *ACS Appl. Mater. Interfaces*, 2014, **6**, 8878.

80 W. Fang, S. Tang, P. Liu, X. Fang, J. Gong and N. Zheng, *Small*, 2012, **8**, 3816–3822.

81 X. Huang, S. Tang, B. Liu, B. Ren and N. Zheng, *Adv. Mater.*, 2011, **23**, 3420–3425.

82 S. Shi, X. Chen, J. Wei, Y. Huang, J. Weng and N. Zheng, *Nanoscale*, 2016, **8**, 5706–5713.

83 E. Hao, K. L. Kelly, J. T. Hupp and G. C. Schatz, *J. Am. Chem. Soc.*, 2002, **124**, 15182–15183.

84 S. Chen and D. L. Carroll, *J. Phys. Chem. B*, 2004, **108**, 5500–5506.

85 S. Chen, Z. Fan and D. L. Carroll, *J. Phys. Chem. B*, 2002, **106**, 10777–10781.

86 X. Wang, D. Yang, L. Chen, B. Liu, Z. Teng, N. He and Z. Wang, *Part. Part. Syst. Charact.*, 2018, **35**, 1800268.

87 G. Zhang, R. Du, J. Qian, X. Zheng, X. Tian, D. Cai, J. He, Y. Wu, W. Huang and Y. Wang, *Nanoscale*, 2017, **10**, 488–498.

2988 | *J. Mater. Chem. B*, 2020, **8**, 2974–2989

This journal is © The Royal Society of Chemistry 2020

88 Y. Lin, Y. Wu, R. Wang, G. Tao, P. F. Luo, X. Lin, G. Huang, J. Li and H. H. Yang, *Chem. Commun.*, 2018, **54**, 8579–8582.

89 H. Lin, W. Qiu, J. Liu, L. Yu, S. Gao, H. Yao, Y. Chen and J. Shi, *Adv. Mater.*, 2019, **31**, 1903013.

90 H. Lin, X. Wang, L. Yu, Y. Chen and J. Shi, *Nano Lett.*, 2017, **17**, 384–391.

91 R. Cai, D. Yang, J. Wu, L. Zhang, C. Wu, X. Chen, Y. Wang, S. Wan, F. Hou and Q. Yan, *Nano Res.*, 2016, 1–11.

92 S. Mitra, H. S. Sasmal, T. Kundu, S. Kandambeth, K. Illath, D. Díaz Díaz and R. Banerjee, *J. Am. Chem. Soc.*, 2017, **139**, 4513–4520.

93 X. Wang, Y. Ma, X. Sheng, Y. Wang and H. Xu, *Nano Lett.*, 2018, **18**, 2217–2225.

94 J. H. Appel, D. O. Li, J. D. Podlevsky, A. Debnath, A. A. Green, Q. H. Wang and J. Chae, *ACS Biomater. Sci. Eng.*, 2016, **2**, 361–367.

95 P. Yuan, Q. Zhou and X. Hu, *Environ. Sci. Technol.*, 2018, **52**, 13543–13552.

96 W. Jiang, B. Y. S. Kim, J. T. Rutka and W. C. W. Chan, *Nat. Nanotechnol.*, 2008, **3**, 145–150.

97 Q. Liu, C. Y. Sun, Q. He, A. Khalil, T. Xiang, D. B. Liu, Y. Zhou, J. Wang and L. Song, *Nano Res.*, 2015, **8**, 3982–3991.

98 E. Chng and M. Pumera, *RSC Adv.*, 2015, **5**, 3074–3080.

99 X. Zhu, X. Ji, N. Kong, Y. Chen, M. Mahmoudi, X. Xu, L. Ding, W. Tao, T. Cai, Y. Li, T. Gan, A. Barrett, Z. Bharwani, H. Chen and O. C. Farokhzad, *ACS Nano*, 2018, **12**, 2922–2938.

100 T. Liu, S. Shi, C. Liang, S. Shen, L. Cheng, C. Wang, X. Song, S. Goel, T. E. Barnhart and W. Cai, *ACS Nano*, 2015, **9**, 950–960.

101 Q. Han, X. Wang, X. Jia, S. Cai, W. Liang, Y. Qin, R. Yang and C. Wang, *Nanoscale*, 2017, **9**, 5927–5934.

102 R. Kurapati, L. Muzi, A. P. R. de Garibay, J. Russier, D. Voiry, I. A. Vacchi, M. Chhowalla and A. Bianco, *Adv. Funct. Mater.*, 2017, **27**, 1605176.

103 C. Wu, S. Wang, J. Zhao, Y. Liu, Y. Zheng, Y. Luo, C. Ye, M. Huang and H. Chen, *Adv. Funct. Mater.*, 2019, **29**, 1901722.

104 J. Hao, G. Song, T. Liu, X. Yi, K. Yang, L. Cheng and Z. Liu, *Adv. Sci.*, 2017, **4**, 1600160.

105 H. Yang, J. Zhao, C. Wu, C. Ye, D. Zou and S. Wang, *Chem. Eng. J.*, 2018, **351**, 548–558.

106 Z. Liu, S. Zhang, H. Lin, M. Zhao, H. Yao, L. Zhang, W. Peng and Y. Chen, *Biomaterials*, 2018, **155**, 54–63.

107 H. Zhang, W. Zeng, C. Pan, L. Feng, M. Ou, X. Zeng, X. Liang, M. Wu, X. Ji and L. Mei, *Adv. Funct. Mater.*, 2019, **29**, 1903791.

108 Y. Zhao, H. Wang, H. Huang, Q. Xiao, Y. Xu, Z. Guo, H. Xie, J. Shao, Z. Sun, W. Han, X.-F. Yu, P. Li and P. K. Chu, *Angew. Chem., Int. Ed.*, 2016, **55**, 5003–5007.

109 J. R. Choi, K. W. Yong, J. Y. Choi, A. Nilghaz, Y. Lin, J. Xu and X. Lu, *Theranostics*, 2018, **8**, 1005–1026.

110 Z. Liu, H. Chen, Y. Jia, W. Zhang, H. Zhao, W. Fan, W. Zhang, H. Zhong, Y. Ni and Z. Guo, *Nanoscale*, 2018, **10**, 18795–18804.

111 X. Mu, J.-Y. Wang, X. Bai, F. Xu, H. Liu, J. Yang, Y. Jing, L. Liu, X. Xue, H. Dai, Q. Liu, Y.-M. Sun, C. Liu and X.-D. Zhang, *ACS Appl. Mater. Interfaces*, 2017, **9**, 20399–20409.

112 M. G. Raucci, I. Fasolino, M. Caporali, M. Serrano-Ruiz, A. Soriente, M. Peruzzini and L. Ambrosio, *ACS Appl. Mater. Interfaces*, 2019, **11**, 9333–9342.

113 X. Zhang, Z. Zhang, S. Zhang, D. Li, W. Ma, C. Ma, F. Wu, Q. Zhao, Q. Yan and B. J. S. Xing, *Adv. Sci.*, 2017, **13**, 1701210.

114 S. J. Song, S. Yong, L. Hyun, K. Bongju, H. Dong-Wook and L. D. J. Nanomaterials, *Nanomaterials*, 2018, **8**, 408.

115 J. Shao, H. Xie, H. Huang, Z. Li, Z. Sun, Y. Xu, Q. Xiao, X.-F. Yu, Y. Zhao, H. Zhang, H. Wang and P. K. Chu, *Nat. Commun.*, 2016, **7**, 12967.

116 W. Zhou, T. Pan, H. Cui, Z. Zhao, P. K. Chu and X.-F. Yu, *Angew. Chem., Int. Ed.*, 2019, **58**, 769–774.

117 R. C. Huxford, J. Della Rocca and W. Lin, *Curr. Opin. Chem. Biol.*, 2010, **14**, 262–268.

118 H. Wang, D. Yu, J. Fang, C. Cao, Z. Liu, J. Ren and X. Qu, *ACS Nano*, 2019, **13**, 9206–9217.

119 D. Wang, J. Zhou, R. Chen, R. Shi, G. Xia, S. Zhou, Z. Liu, N. Zhang, H. Wang, Z. Guo and Q. Chen, *Biomaterials*, 2016, **107**, 88–101.

120 X. Qin, L. Cai, H. Zhao, J. Tang, Y. Shen, X. Hu and H. Zeng, *Biosens. Bioelectron.*, 2015, **63**, 294–300.

121 X. G. Luan, Y. Zou, X. Hai, H. Bai, Q. Zhang, R. Riedel and L. Cheng, *J. Eur. Ceram. Soc.*, 2018, **38**, 3804–3813.

122 R. Kurapati, C. Backes, C. Ménard-Moyon, J. N. Coleman and A. Bianco, *Angew. Chem., Int. Ed.*, 2016, **55**, 5506–5511.

123 O. Sen, M. Emanet and M. Culha, *Front. Bioeng. Biotechnol.*, 2018, **6**, 83.

124 K. Zeng, Q. Xu, J. Ouyang, Y. Han, J. Sheng, M. Wen, W. Chen and Y.-N. Liu, *ACS Appl. Mater. Interfaces*, 2019, **11**, 6840–6849.

125 D. Granchi, L. M. Savarino, G. Ciapetti and N. Baldini, *Crit. Rev. Toxicol.*, 2018, **48**, 170–193.

126 I. R. Suhito, Y. Han, D.-S. Kim, H. Son and T.-H. Kim, *Biochem. Biophys. Res. Commun.*, 2017, **493**, 578–584.

This journal is © The Royal Society of Chemistry 2020

J. Mater. Chem. B, 2020, **8**, 2974–2989 | **2989**